nature materials

Article

https://doi.org/10.1038/s41563-024-01908-x

Engineered matrices reveal stiffness-mediated chemoresistance in patient-derived pancreatic cancer organoids

Received: 25 April 2022

Accepted: 30 April 2024

Published online: 04 July 2024

Check for updates

Bauer L. LeSavage[1], Daiyao Zhang[2,11], Carla Huerta-López[3,11], Aidan E. Gilchrist[3,11], Brad A. Krajina[2], Kasper Karlsson[4,5,6], Amber R. Smith[7], Kremena Karagyozova[6], Katarina C. Klett[8], Michelle S. Huang[2], Christopher Long[3], Gernot Kaber[9], Christopher M. Madl[1,10], Paul L. Bollyky[9], Christina Curtis[4,5,6], Calvin J. Kuo[7] & Sarah C. Heilshorn[3]

Pancreatic ductal adenocarcinoma (PDAC) is characterized by its fibrotic and stiff extracellular matrix. However, how the altered cell/extracellular-matrix signalling contributes to the PDAC tumour phenotype has been difficult to dissect. Here we design and engineer matrices that recapitulate the key hallmarks of the PDAC tumour extracellular matrix to address this knowledge gap. We show that patient-derived PDAC organoids from three patients develop resistance to several clinically relevant chemotherapies when cultured within high-stiffness matrices mechanically matched to in vivo tumours. Using genetic barcoding, we find that while matrix-specific clonal selection occurs, cellular heterogeneity is not the main driver of chemoresistance. Instead, matrix-induced chemoresistance occurs within a stiff environment due to the increased expression of drug efflux transporters mediated by CD44 receptor interactions with hyaluronan. Moreover, PDAC chemoresistance is reversible following transfer from high- to low-stiffness matrices, suggesting that targeting the fibrotic extracellular matrix may sensitize chemoresistant tumours. Overall, our findings support the potential of engineered matrices and patient-derived organoids for elucidating extracellular matrix contributions to human disease pathophysiology.

Pancreatic ductal adenocarcinoma (PDAC) is a lethal disease with an overall five-year survival rate of less than 7% (refs. 1,2). Front-line chemotherapeutics to treat PDAC are often ineffective due to intrinsic or acquired resistance[3], and no approved chemotherapies have substantially extended PDAC patient survival since the regulatory approval of gemcitabine in 1996 (refs. 4,5). Therefore, understanding the mechanisms of how PDAC tumours develop and retain chemoresistance is critical to advancing impactful treatment strategies.

Clinically, PDAC chemoresistance has been correlated with extreme fibrotic remodelling of the extracellular matrix (ECM)[6,7]. Moreover, several ECM components secreted by both PDAC and stromal cells have been found to correlate with poor patient survival[8]. The PDAC ECM is characterized by its high stiffness and dense stroma, which worsens throughout disease progression[6,7]. In PDAC, these matrix properties and the associated high interstitial fluid pressures are largely thought to impact chemoresistance by acting as a physical barrier that limits drug delivery to the tumour[9]. Promisingly, recent PDAC studies have shown that co-administration of chemotherapies and ECM-depleting factors can significantly improve survival rates in mice[9,10]. However, these therapies based on animal models have yet

A full list of affiliations appears at the end of the paper. e-mail: heilshorn@stanford.edu

to show efficacy in human PDAC trials[11,12], suggesting the ECM may be playing additional roles in driving PDAC chemoresistance.

As these fibrotic ECM properties are known to directly influence cancer cell phenotypes in other tumour types[13–15], we hypothesized that the PDAC ECM might drive chemoresistance through direct cell–ECM signalling. Human cancer organoids offer a relatively cost-effective and representative model of patient-specific tumours and their matrix[16–19]. However, traditional methods for culturing cancer organoids in vitro rely on animal-derived ECMs such as basement membrane extract (for example, Matrigel/Cultrex) that are ill-defined and non-tunable[16,20], which limits the ability to uncover mechanistic links between ECM properties and chemoresistance. Notably, Matrigel alternatives are currently being explored for organoid models[21–25] yet have not been applied to understanding matrix-mediated PDAC chemoresistance in human-specific models.

Here we engineer a defined and tunable three-dimensional (3D) matrix that mimics key biochemical and mechanical properties of the in vivo PDAC ECM and supports the long-term culture and passaging of human, patient-derived PDAC organoids in vitro. Using our engineered matrix, we identify previously untested causal relationships between PDAC chemoresistance and the ECM, which opens new directions of drug development for effective patient therapy.

ECM stiffness drives PDAC chemoresistance

The in vivo PDAC ECM is characterized by the increased deposition of several matrix components including fibronectin and hyaluronan (HA)[6,7] (Fig. 1a and Supplementary Fig. 1). RNA-sequencing (RNA-seq) analysis of 179 PDAC and 171 normal pancreas tissues collected from The Cancer Genome Atlas and Genome-Tissue Expression Project[26] confirmed increased expression of fibronectin (*FN1*) and HA synthesis (*HAS1*, *HAS2*, *HAS3*, *UGDH*) genes (Fig. 1b). Increased matrix deposition also correlated with the increased tumour stiffness (~2,900 Pa) of freshly resected human samples compared to normal pancreas tissue (~900 Pa; Fig. 1c).

To model these biochemical components and mechanical features of the PDAC ECM in vitro, we designed a defined and tunable 3D matrix composed of HA and elastin-like protein (ELP), which we term HELP[22] (Fig. 1d). ELP is a recombinant protein consisting of repeating elastin-derived and fibronectin-derived sequences that include an arginylglycylaspartic acid (RGD)–integrin binding motif[27]. By tuning the polymer concentration and chemical cross-link density between benzaldehyde and hydrazine groups on the HA and ELP, respectively, we created a physiologically relevant range of HELP matrices that span from the low stiffness of Cultrex hydrogel controls to the high stiffness of PDAC tumour tissue (Fig. 1e and Supplementary Figs. 2 and 3), while maintaining identical HA content (10 mg ml^{-1}) and RGD concentration (1 mM; Supplementary Tables 1 and 2). We termed these formulations HELP Low, HELP Medium and HELP High, corresponding to their stiffness. By comparison, Cultrex is a complex mixture of multiple peptides and matrix proteins derived from the reconstituted basement membrane of mouse sarcoma[20], with minimal HA (Supplementary Fig. 4).

For all hydrogel encapsulations, patient-derived PDAC organoids were dissociated into single-cell suspensions and encapsulated within either Cultrex or HELP matrices of varying stiffness. Organoids showed robust expansion in all matrices and stained positive for cytokeratin 19 (ductal lineage) and KI67 (proliferation) proteins (Fig. 1f). PDAC organoids encapsulated in HELP matrices had an initial delay in proliferation compared to Cultrex hydrogels, yet exhibited a similar overall diameter growth rate over 7–14 days (Fig. 1g and Supplementary Fig. 5a,b).

To test how matrix properties impact PDAC drug sensitivity, we treated ~75-µm-diameter PDAC organoids with 100 nM gemcitabine, a nucleoside analogue commonly prescribed for clinical treatment of PDAC tumours[5], for three days. We found organoids cultured in HELP High matrices had lower levels of the apoptotic marker cleaved caspase 3 and were more resistant to gemcitabine treatment compared to HELP Low and Cultrex matrices (Fig. 1h,i).

In agreement with Ki67 and organoid diameter data, cell cycle analysis of the organoids showed no significant difference in the percentage of proliferative cells in the S phase when grown within each matrix (Supplementary Figs. 5–7). Additionally, all hydrogels had a similar microstructure and diffusion of macromolecules ranging in size from 10–250 kDa, ensuring no differences in gemcitabine (263 Da) delivery to organoids grown in different matrices (Supplementary Fig. 8). From these data, we concluded that matrix interactions are a key driver of PDAC organoid chemoresistance in our model.

Long-term culture in stiff matrix drives chemoresistance

To explore the dynamic onset of PDAC chemoresistance over long-term exposure to high stiffness, we cultured PDAC organoids in HELP Low or HELP High matrices and tested their drug sensitivity on a subset of previously untreated cells following one and four passages. Specifically, cells were treated with gemcitabine following the formation of ~75-µm-diameter organoids (Fig. 2a). Interestingly, after four passages within HELP High, PDAC organoids showed increased resistance to gemcitabine compared to treatment during passage 1, resulting in a doubling of the half-maximal inhibitory concentration (IC_{50}) value (Fig. 2b,c). Expansion of PDAC organoids in HELP Low and Cultrex matrices for four passages did not result in a statistically significant difference in gemcitabine IC_{50} (Fig. 2b,c and Supplementary Fig. 9).

To test whether drug response was dependent on the stage of organoid formation and to further validate these results using a second, complementary assay, we treated PDAC cells with gemcitabine during log-phase growth of single cells following either one or four passages

Fig. 1 | ECM stiffness drives PDAC chemoresistance. a, Representative immunofluorescence images of human PDAC and normal adjacent pancreatic tissue stained for ECM components. Scale bars, 100 µm. **b**, Bulk RNA-seq analysis of PDAC and normal pancreatic tissue for fibronectin (*FN1*) and HA-associated (*HAS1*, *HAS2*, *HAS3*, *UGDH*) genes ($N = 179$ for PDAC, $N = 171$ for normal). Box plot represents the 25th, 50th and 75th percentiles; upper and lower whiskers represent ×1.5 interquartile range; all data points shown. TPM, transcripts per million. **c**, Stiffness measurements of fresh, surgically resected human PDAC and normal pancreatic tissue ($N = 5$ or 6 independent biological replicates, mean ± s.d., unpaired two-tailed *t*-test, $^{****}P < 0.0001$). **d**, Schematic of engineered HELP matrix. **e**, Stiffness measurements of Cultrex and HELP matrices ($N = 4$–6 independent experimental replicate hydrogels, mean ± s.d., ordinary one-way analysis of variance (ANOVA) with Tukey multiple comparisons correction; NS, not significant). Low, Medium or High labels refer to relative stiffness values. **f**, Representative bright-field (top) and immunofluorescence (bottom) images of PDAC organoids cultured within Cultrex and HELP matrices. Bright-field scale bars, 250 µm; immunofluorescence scale bars, 50 µm. **g**, Quantification of PDAC organoid diameter during culture within Cultrex and HELP matrices. Each data point represents the average organoid diameter from one hydrogel at the given time point ($N = 3$ independent experimental replicate hydrogels; Cultrex, $n = 77$–164; HELP Low, $n = 84$–206; HELP Medium, $n = 93$–284; HELP High, $n = 85$–223 organoids per individual hydrogel per time point). No statistical difference measured across HELP matrices at each time point using ordinary one-way ANOVA with Tukey multiple comparisons correction. Dashed line represents approximate organoid diameter where cultures are confluent. **h**, Representative immunofluorescence images of PDAC organoids cultured within Cultrex and HELP matrices and treated with DMSO control (inset) or 100 nM gemcitabine for 3 days following organoid formation (cleaved caspase 3 is the apoptosis marker). Scale bars, 50 µm. F-actin, filamentous actin. **i**, Quantification of cleaved caspase 3 signal normalized to DMSO control. Each data point represents the average cleaved caspase 3 area per nuclei from one confocal *z* stack containing several organoids ($N = 3$ independent experimental replicate hydrogels, $n = 5$–8 *z* stacks per hydrogel, geometric mean ± 95% confidence interval, ordinary one-way ANOVA with Tukey multiple comparisons correction, $^{*}P < 0.05$, $^{**}P < 0.01$, $^{***}P < 0.001$).

https://doi.org/10.1038/s41563-024-01908-x

(Fig. 2d). Following four passages in HELP High matrices, PDAC single cells adopted the same stiffness-mediated chemoresistance as seen with multicellular organoid drug treatment, while cells expanded in HELP Low or Cultrex matrices did not significantly increase their IC_{50} value (Fig. 2e,f and Supplementary Fig. 9).

Furthermore, similar results were obtained for two additional front-line chemotherapy treatments, paclitaxel and a combination of fluorouracil, irinotecan and oxaliplatin (three cancer-cell-targeting drugs in the regimen FOLFIRINOX), where more chemoresistance was observed in stiffer matrices (Fig. 2g,h and Supplementary Fig. 10). Finally, similar results were obtained for two additional PDAC patient-derived samples (Fig. 2i–k and Supplementary Table 3), while no matrix-induced chemoresistance was observed for patient cells from a different type of pancreatic cancer (primary solid pseudopapillary neoplasm; Supplementary Fig. 11). Taken together, these data show that matrix-mediated chemoresistance is observed across a range of treatment regimens and patient organoid lines. Moreover, these results led us to form and test two alternative mechanistic hypotheses for the

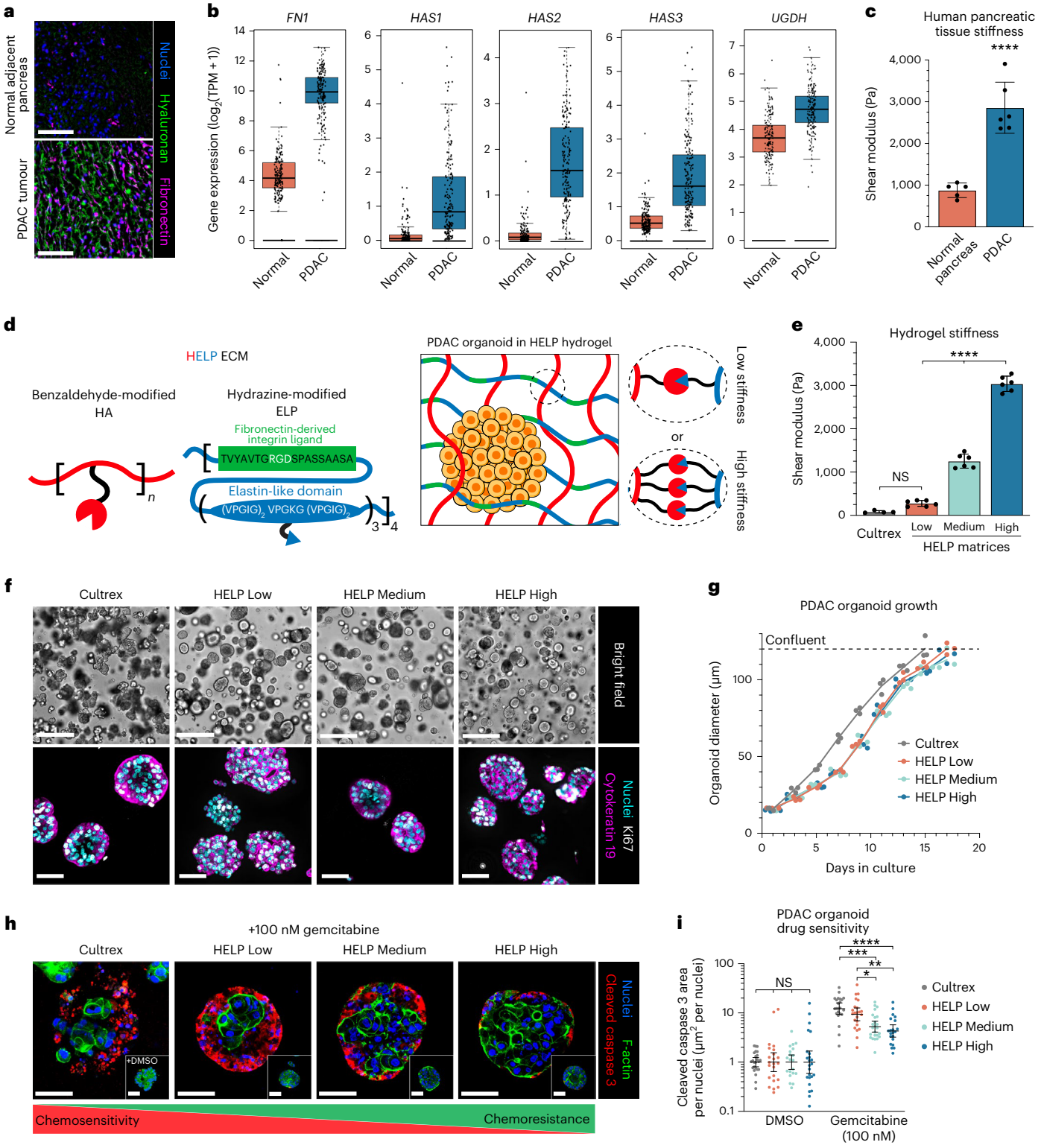

https://doi.org/10.1038/s41563-024-01908-x

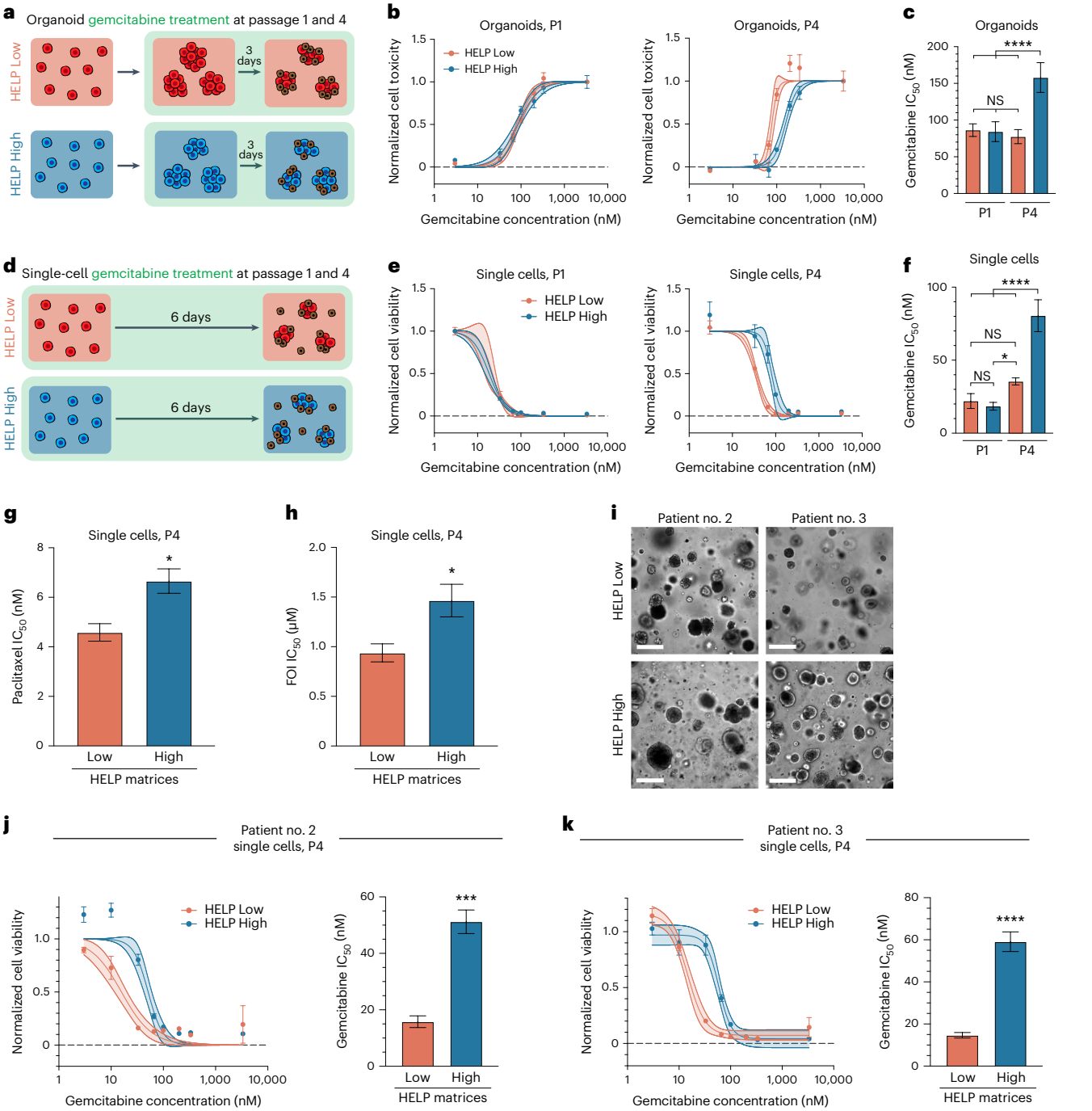

Fig. 2 | Long-term culture in stiff matrices drives PDAC chemoresistance. **a**, Schematic of PDAC organoid drug treatment protocol, where cultures are treated with gemcitabine for 3 days following the formation of ~75-μm-diameter organoids. **b**, Organoid-level gemcitabine dose–response curves for PDAC organoids from patient number 1 expanded within HELP Low and HELP High matrices for passage 1 (P1, left) or passage 4 (P4, right). **c**, Gemcitabine IC_{50} values calculated from nonlinear fit of dose–response curves shown in **b**. **d**, Schematic of single-cell drug treatment protocol, where PDAC cultures are treated with gemcitabine for six days during log-phase growth of single cells. **e**, Single-cell-level gemcitabine dose–response curves for PDAC organoids from patient number 1 expanded within HELP Low and HELP High matrices for one (left) or four (right) passages. **f**, Gemcitabine IC_{50} values calculated from nonlinear fit of dose–response curves shown in **e**. **g**,**h**, Paclitaxel (**g**) and FOI (**h**) IC_{50} values calculated from nonlinear fit of single-cell-level dose–response curves for patient number 1. FOI refers to fluorouracil, oxaliplatin and irinotecan added in molar concentration ratios of 1:1:0.001, respectively. Reported concentrations for FOI are the concentrations of fluorouracil/oxaliplatin. Data are mean ± s.e.m. ($N = 3$ or 4 independent experimental replicate hydrogels, unpaired two-tailed t-test, $^{*}P < 0.05$). **i**, Representative bright-field images of patient numbers 2 and 3 within HELP Low and HELP High matrices for four passages. Scale bar is 250 μm. **j**,**k**, Single-cell-level gemcitabine dose–response curves and calculated IC_{50} values for PDAC organoids from patient number 2 (**j**) and patient number 3 (**k**) expanded in HELP Low and HELP High matrices for four passages. In **b**, **e**, **j** and **k**, each data point represents the mean ± s.e.m. ($N = 3$ or 4 independent experimental replicate hydrogels; solid centre line is nonlinear least squares regression of data; shaded region represents 95% confidence bands of nonlinear fit; data are normalized to DMSO or 3 nM gemcitabine for single cells or 3,333 nM gemcitabine for organoids). In **c** and **f**, each bar represents the mean ± s.e.m. ($N = 3$ or 4 independent experimental replicate hydrogels, ordinary one-way ANOVA with Tukey multiple comparisons correction, $^{****}P < 0.0001$). In **j** and **k**, each bar represents the mean ± s.e.m. ($N = 3$ or 4 independent experimental replicate hydrogels, unpaired two-tailed t-test, $^{***}P < 0.001$).

initiation of matrix-induced chemoresistance: (1) the genetic clonal selection for chemoresistant genotypes, and (2) the phenotypic shift of cells towards more chemoresistant phenotypes.

Matrix stiffness mediates organoid clonal heterogeneity

PDAC tumours are characterized by their substantial intratumoural heterogeneity and the existence of clonal populations that may uniquely respond to treatment[28]. Given that organoid models can retain cellular heterogeneity in vitro[29,30] and that our chemoresistant phenotype is preserved on the single-cell level, we hypothesized that stiffness-mediated chemoresistance could be due to the selection of inherently resistant subclones within our organoid population. To explore this hypothesis, we cultured genetically barcoded[31] PDAC organoids from patient number 1 within the Cultrex, HELP Low and HELP High matrices for three passages (Extended Data Fig. 1a). Following each passage, a subset of organoids from each matrix condition was collected for barcode sequencing to track the relative frequencies of each clone over time. Our results show that PDAC organoids cultured within HELP High matrices had steeper clonal selection over three passages compared to HELP Low and Cultrex matrices (Extended Data Fig. 1b,c and Supplementary Fig. 12).

To identify whether the enriched clones in HELP High were unique across matrices, we quantified the overlap of barcodes and their relative frequencies following three passages. We found each matrix enriched a subset of barcodes unique to only that matrix (Extended Data Fig. 1d) and that several clones preferred expanding in either a low- or high-stiffness environment, suggesting that distinct cancer subclones exhibit different fitnesses in response to matrix properties (Supplementary Figs. 13 and 14).

Despite this preference for specific matrices by some subclones, the majority of subclone barcodes in HELP High were also present in the HELP Low and Cultrex matrices (88% and 92% overlap, respectively; Extended Data Fig. 1d and Supplementary Fig. 15). Moreover, the frequency of the 15 barcodes unique to HELP High were relatively low, and their cumulative frequency accounted for <1% of the total population (Extended Data Fig. 1d,e), suggesting these clones have not sufficiently expanded to drive broad changes in gemcitabine IC_{50}. In addition, the frequency of clones in HELP High was highly correlated with that in the HELP Low and Cultrex matrices (Extended Data Fig. 1f). Overall, these data suggest the HELP High matrices did not enrich for an inherently chemoresistant subpopulation and that PDAC organoids may instead be altering their phenotype in response to the matrix stiffness.

Drug efflux transporters mediate PDAC chemoresistance

To test our second hypothesis, that matrix-mediated drug sensitivity is driven by a plastic organoid phenotype instead of the expansion of unique, inherently chemoresistant cellular genotypes, we examined the expression of protein markers correlated with chemoresistance. For example, increased protein expression of cell-surface drug efflux transporters can result in greater chemoresistance by dynamically pumping therapeutics out of cancer cells[32–34]. In particular, the ATP-binding cassette (ABC) family of drug efflux transporters has been recognized as a chemoresistance mechanism in a variety of cancers, including PDAC[35]. Therefore, understanding the environmental cues that mediate the expression, maintenance and activity of ABC-family drug transporters could potentially lead to new treatment strategies to sensitize patient tumours.

We found that several ABC-family drug efflux transporters commonly associated with PDAC and/or gemcitabine resistance[36–41] (*ABCG2*, *ABCC3*, *ABCC4*, *ABCC5*) were upregulated in organoids in stiff HELP High matrices compared to in HELP Low and Cultrex (Fig. 3a and Supplementary Figs. 16a and 17). Solute carrier (SLC)-family concentrative and equilibrative transporters associated with gemcitabine influx[3] (*SLC28A1*, *SLC28A3*, *SLC29A1*, *SLC29A2*) were either not influenced by matrix stiffness or showed a modest increase in HELP High (Fig. 3b and Supplementary Fig. 16b). Specifically, the drug efflux transporter ABCG2, also known as breast cancer resistance protein, has previously been connected to multidrug resistance in pancreatic cancer[36]. Notably, PDAC organoids grown in stiff HELP High matrices had higher protein expression of ABCG2 compared to HELP Low (Fig. 3c,d).

We next performed a side population (SP) assay to quantify the functional activity of drug efflux transporters[42]. Following expansion of PDAC organoids for four passages in HELP Low, HELP High or Cultrex matrices, organoids were dissociated into single cells and treated with Hoechst 33342, a live-cell-permeable DNA stain. As several ABC-family transporters, including ABCG2, have been shown to readily efflux Hoechst, cells with a higher efflux pump activity should show a decreased fluorescent signal when measured via flow cytometry[42,43] (Fig. 3e,f).

We found organoids cultured in HELP High had a significantly larger SP compared to HELP Low in all three patients (Fig. 3g,h and Supplementary Figs. 18–22). To test the specific role of ABCG2 in mediating this response, we performed the same SP assay with the addition of Ko143 (CAS number 461054-93-3), a small-molecule inhibitor with strong affinity to the ABCG2 transporter[44]. Treatment with Ko143 for two hours led to a significant decrease in SP across all three organoid lines cultured in both HELP High and Low (Fig. 3g,h and Supplementary Figs. 18–22), highlighting ABCG2 as a highly active efflux transporter for PDAC organoids. Similar treatment with verapamil, a less-specific ABC-family transport inhibitor[38,42], also led to a decrease in SP (Supplementary Figs. 18, 19 and 22). Organoids grown within Cultrex also showed a similar decrease in SP (Supplementary Figs. 22 and 23).

To functionally test if SP cells display increased chemoresistance, SP cells were sorted via fluorescence-activated cell sorting (FACS) and collected for further analysis. SP cells, G0/G1 phase cells and a control

Fig. 3 | Drug efflux transporter expression and activity mediates PDAC organoid chemoresistance. a,**b**, ABC-family (**a**) and SLC-family (**b**) drug transporter mRNA quantification in PDAC organoids expanded within HELP Low or HELP High for four passages ($N = 4$ independent experimental replicate hydrogels, mean ± 95% confidence interval, two-tailed t-test comparing HELP Low and HELP High, $^{*}P < 0.05$, $^{**}P < 0.01$, $^{***}P < 0.001$). Data are normalized to *GAPDH* and respective marker expression in organoids expanded within Cultrex. **c**, Representative immunofluorescence images of ABCG2 in PDAC organoids expanded within HELP Low and HELP High. Scale bars are 100 µm. **d**, Representative flow cytometry analysis of ABCG2 expression in PDAC organoids expanded within HELP Low and HELP High (representative of $N = 3$ independent experimental replicates). **e**, Summary of drug transporter expression and predicted efflux of Hoechst. **f**, Schematic of SP results via flow cytometry. G2/M refers to the G2/mitosis phases of the cell cycle. Apo, apoptosis. **g**, Representative SP flow cytometry analysis of PDAC organoids expanded within HELP Low (left) or HELP High (right) for four passages and treated with Hoechst (top) or Hoechst + Ko143 (ABCG2 efflux transporter inhibitor; bottom) for 2 h (representative of $N = 3$ independent experimental replicates). SP is outlined in black with the SP percentage at the top. **h**, Quantification of SP percentage from the full dataset represented in **g** ($N = 3$ independent experimental replicates; connected data points are from the same parent population). Statistical analysis was performed using a paired t-test (control versus Ko143 for each matrix; $P = 0.050$) or a two-tailed t-test (percentage of SP cells across controls). **i**, Schematic summarizing the experiment to test the SP's propensity for increased organoid reformation and drug resistance. **j**, Bright-field images of PDAC organoids grown within Cultrex for nine days following FACS sorting into distinct populations. Scale bars are 300 µm. **k**, Post-sorted PDAC organoid viability following treatment with gemcitabine ($N = 4$ independent experimental replicate hydrogels, mean ± s.d.). PDAC organoids were grown in Cultrex for three days prior to gemcitabine treatment for six days during log-phase growth. Statistical analysis was performed using an ordinary one-way ANOVA with Tukey multiple comparisons correction, $^{****}P < 0.0001$.

https://doi.org/10.1038/s41563-024-01908-x

of cells gated only on viability were grown in Cultrex and treated with either dimethyl sulfoxide (DMSO) or 50 nM gemcitabine (Fig. 3i and Supplementary Fig. 24). After nine days of culture, SP cells were more chemoresistant to gemcitabine treatment compared to G0/G1 cells and the viable control population (Fig. 3j,k), consistent with our hypothesis that increased function of efflux pumps can lead to increased chemoresistance.

Long-term drug efflux inhibition increases chemoresistance

Due to their ability to block drug efflux pumps that may enable chemoresistance in cancer cells, inhibitors like Ko143 and verapamil have been explored as a potential treatment strategy to sensitize tumours to chemotherapy[32,35,44]. Therefore, we hypothesized that co-administration of gemcitabine and Ko143 in vitro would lead to

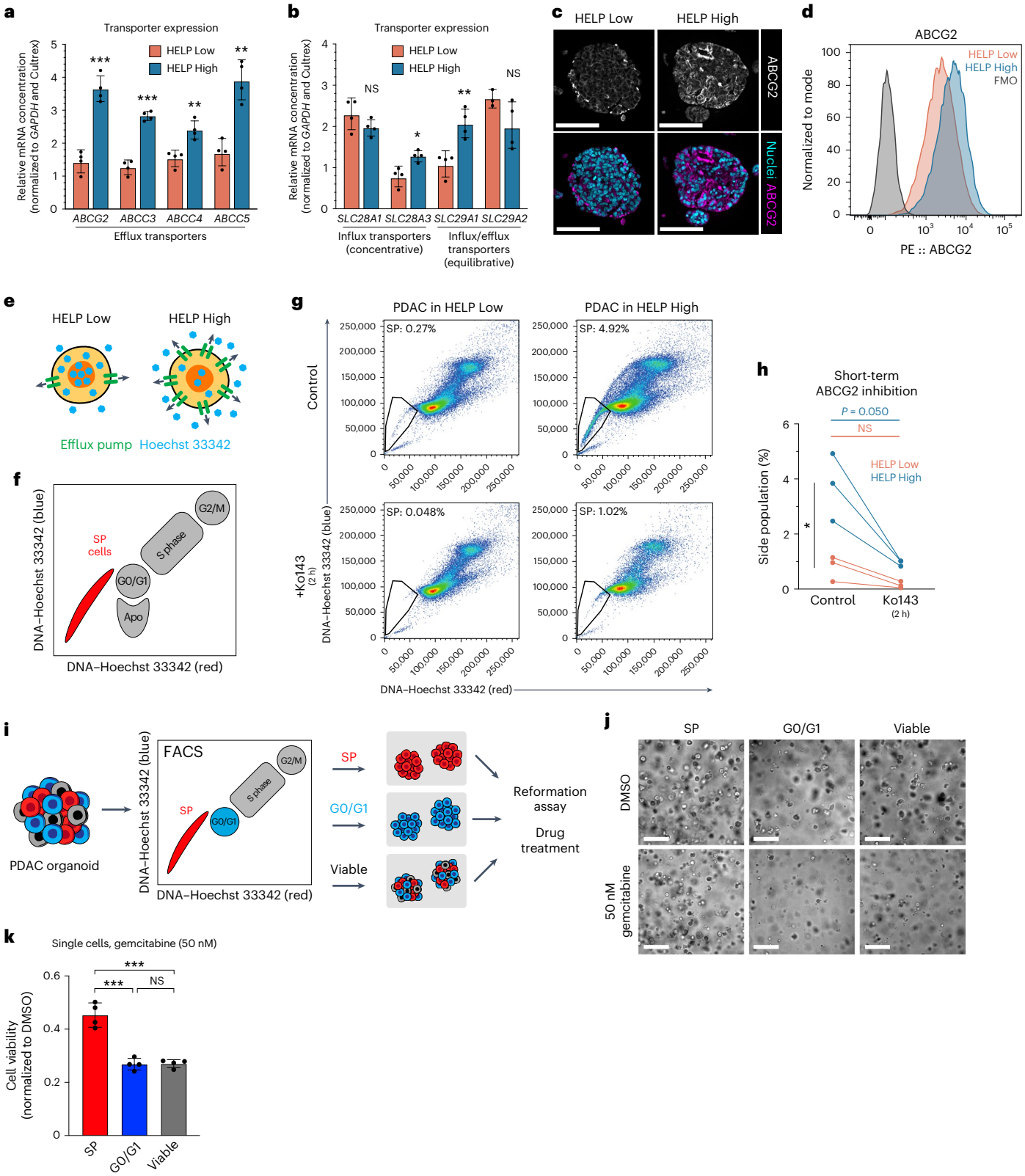

https://doi.org/10.1038/s41563-024-01908-x

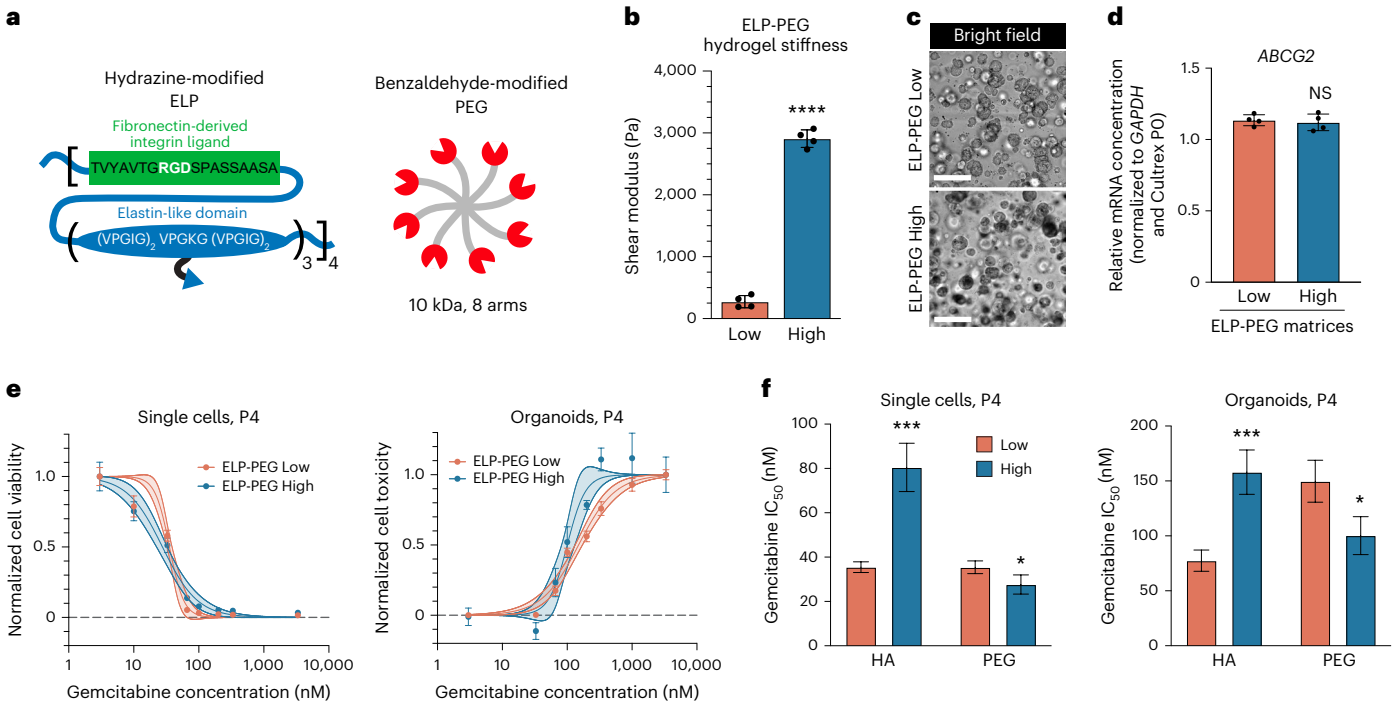

Fig. 4 | Influence of HA on PDAC chemoresistance. a, Schematic of ELP-PEG matrix, where HA has been replaced with inert PEG, resulting in a matrix without HA, but with identical mechanical properties and RGD concentration to HELP. **b**, Stiffness measurements of ELP-PEG matrices, stiffness-matched to HELP Low and HELP High ($N = 4$ independent experimental replicate hydrogels, mean ± s.d., unpaired two-tailed t-test, $^{****}P < 0.0001$). **c**, Representative bright-field images of PDAC organoids expanded within ELP-PEG Low (top) or ELP-PEG High (bottom) for four passages. Scale bars, 250 µm. **d**, Quantitative polymerase chain reaction (qPCR) quantification of mRNA-level *ABCG2* expression in PDAC organoids expanded within ELP-PEG Low or High for four passages ($N = 4$ independent experimental replicate hydrogels, mean ± 95% confidence interval). Statistical analysis comparing marker expression in Low versus High matrices was performed using an unpaired two-tailed t-test. All data are normalized to *GAPDH* gene expression and respective marker expression in the PDAC organoid parent population cultured within Cultrex prior to expansion in ELP-PEG (that is, Cultrex P0). **e**, Single-cell-level (left) and organoid-level (right) gemcitabine dose–response curves for PDAC organoids expanded within ELP-PEG Low or High for four passages. Each data point represents the mean ± s.e.m. ($N = 4$ independent experimental replicate hydrogels; solid centre line is nonlinear least squares regression of data; shaded region represents 95% confidence bands of nonlinear fit; data are normalized to 3 nM gemcitabine for single cells or 3,333 nM gemcitabine for organoids). **f**, Gemcitabine IC_{50} values calculated from nonlinear fit of dose–response curves shown in **e** for single-cell (left) and organoid (right) drug treatment in ELP-PEG compared to HELP containing HA. Each bar represents the mean ± s.e.m. ($N = 4$ independent experimental replicate hydrogels, unpaired two-tailed t-test between Low and High for each matrix variation, $^{*}P < 0.05$, $^{***}P < 0.001$).

increased drug sensitivity of PDAC organoids and overall reduced cell survival.

Surprisingly, we found that the long-term addition of Ko143 throughout our six-day single-cell and three-day organoid drug treatment protocols decreased sensitivity to gemcitabine and promoted PDAC survival across HELP matrices, with a stronger effect seen in HELP High (Extended Data Fig. 2a–c and Supplementary Fig. 25a). In agreement with SP data, organoids within Cultrex showed a similar response to long-term Ko143 treatment (Supplementary Fig. 25b,c). Importantly, Ko143 treatment alone did not increase cell viability compared to a DMSO control (Supplementary Fig. 25d). Similar results were observed with the long-term addition of verapamil, a broad inhibitor of ABC-family transporters (Supplementary Fig. 25e,f).

To explore how long-term Ko143 treatment resulted in increased PDAC organoid chemoresistance, we measured the expression of several drug transporters. Interestingly, we found the addition of Ko143 alone throughout organoid formation led to broad messenger RNA (mRNA)-level and protein-level upregulation of efflux transporters compared to DMSO controls (Extended Data Fig. 2d,e and Supplementary Fig. 26a–e). Similar results were seen for SLC-family concentrative and equilibrative transporters, albeit to a lesser extent than ABC-family efflux pumps (Supplementary Fig. 26f). Overall, our data suggest that PDAC cells compensate for efflux pump inhibition by driving the expression of broad efflux transporters, resulting in increased chemoresistance (Extended Data Fig. 2f).

HA mediates PDAC chemoresistance in stiff matrices

To elucidate the mechanism of increased ABCG2 expression and chemoresistance in our PDAC organoids, we explored the role of specific matrix ligands by leveraging the tunability of our engineered matrix. The PDAC ECM is a dynamic milieu composed of several polymer components including fibronectin and HA, which mediate cancer-cell/ECM interactions through integrin and CD44 engagement, respectively. Furthermore, integrins and CD44 are known to transduce mechanosignalling[45,46]. In particular, the fibronectin-mimicking RGD ligand has been implicated in mediating both cancer progression and drug sensitivity in several cancer types[47].

To explore the role of RGD signalling in our system, we modified the amino acid sequence of our recombinant ELP to present a scrambled, non-integrin-binding RDG motif[22,27], resulting in identical, stiffness-matched HELP Low and High matrices with 0 mM RGD (Extended Data Fig. 3a,b). We found PDAC organoids grew robustly from single-cell encapsulation in HELP RDG Low and HELP RDG High matrices without the RGD ligand (Extended Data Fig. 3c and Supplementary Fig. 27a), and organoids showed similar expression of RGD-binding cell-surface integrins across matrix formulations (Supplementary Fig. 28). *ABCG2* was similarly upregulated in HELP RDG High compared to HELP RDG Low after four passages (Extended Data Fig. 3d).

Furthermore, while HELP RDG High still promoted a chemoresistant phenotype compared to HELP RDG Low, the overall gemcitabine

https://doi.org/10.1038/s41563-024-01908-x

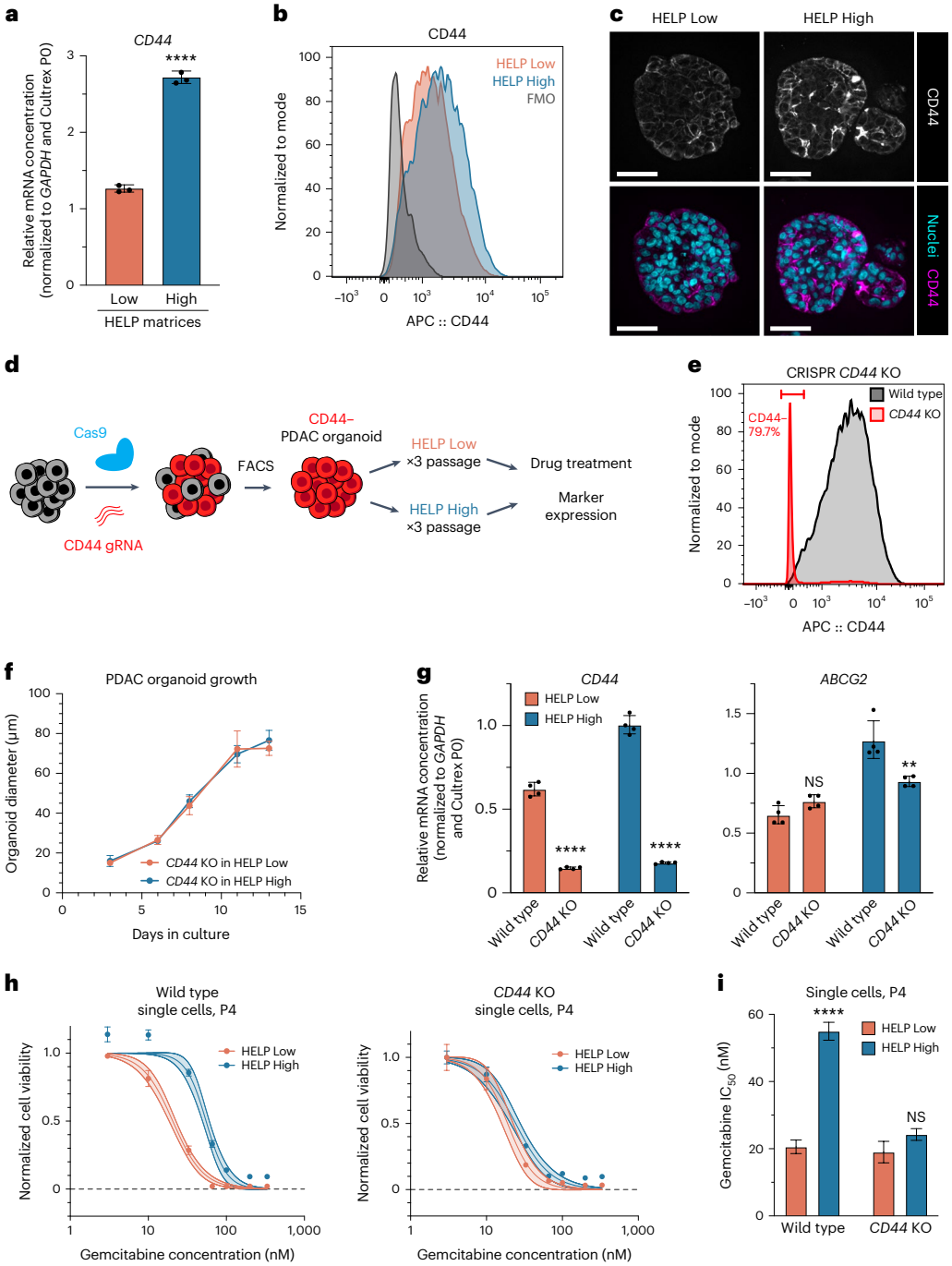

Fig. 5 | HA-mediated CD44 signalling mediates PDAC organoid chemoresistance. a, *CD44* mRNA expression in wild-type PDAC organoids expanded within HELP Low or HELP High for four passages ($N = 3$ independent experimental replicate hydrogels, mean ± 95% confidence interval, unpaired two-tailed *t*-test, $^{****}P < 0.0001$). Data are normalized to *GAPDH* and *CD44* expression in the PDAC organoid parent population cultured within Cultrex (that is, Cultrex P0). **b**, Representative flow cytometry of CD44 expression in PDAC organoids expanded within HELP Low and HELP High (representative of $N = 3$ independent experimental replicates). **c**, Representative immunofluorescence images of CD44 in PDAC organoids expanded within HELP Low and HELP High. Scale bar is 50 µm. **d**, Schematic of method for *CD44* KO via CRISPR-Cas9. gRNA, guide RNA. **e**, Representative flow cytometry of CD44 expression in *CD44* KO and wild-type cells. **f**, Quantification of *CD44* KO PDAC organoid diameter during culture within HELP Low and HELP High. Each data point represents the average organoid diameter at the given time point ($N = 6$ independent experimental replicate hydrogels, mean ± 95% confidence interval; HELP Low, $n = 121–540$ organoids; HELP High, $n = 167–691$ organoids per time point). No statistical difference was measured across HELP matrices of varying stiffness at each time point using unpaired two-tailed *t*-test. **g**, *CD44* (left) and *ABCG2* (right) mRNA expression in wild-type or *CD44* KO PDAC organoids expanded within HELP Low or High for four passages ($N = 4$ independent experimental replicate hydrogels, mean ± 95% confidence interval, unpaired two-tailed *t*-test between wild-type and *CD44* KO for each matrix, $^{**}P < 0.01$). **h**, Single-cell gemcitabine dose–response curves for PDAC *CD44* KO and PDAC wild-type cells expanded within HELP Low and HELP High for four passages. Each data point represents mean ± s.e.m. ($N = 4$ independent experimental replicate hydrogels, solid centre line is nonlinear least squares regression of data; shaded region represents 95% confidence bands of nonlinear fit; data are normalized to DMSO (wild type) or 3 nM gemcitabine (*CD44* KO). **i**, Gemcitabine IC_{50} values calculated from nonlinear fit of dose–response curves shown in **i**. Each bar represents the mean ± s.e.m. ($N = 4$ independent experimental replicate hydrogels, unpaired two-tailed *t*-test between HELP Low and High for each PDAC condition).

https://doi.org/10.1038/s41563-024-01908-x

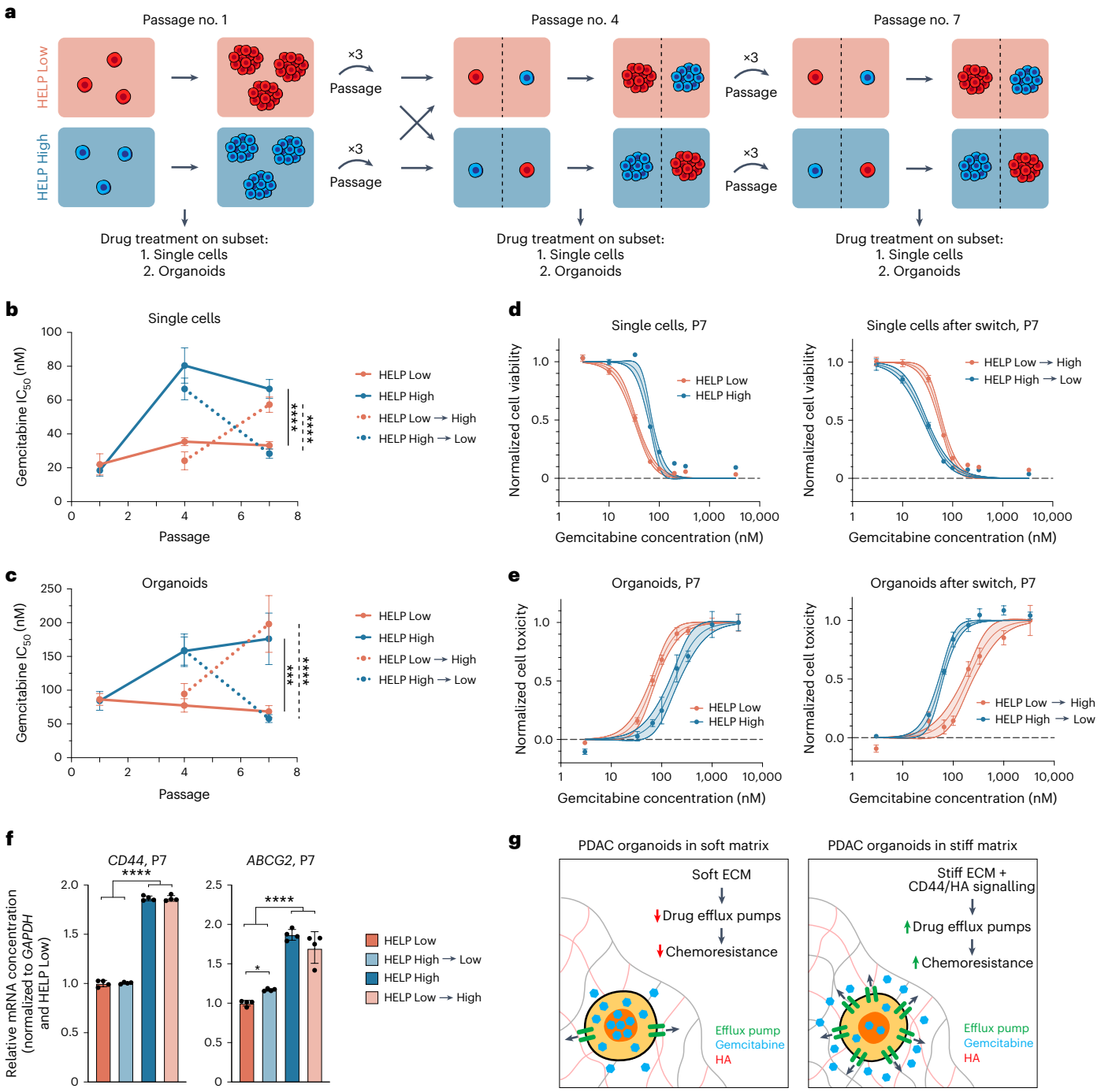

Fig. 6 | Stiffness-mediated PDAC chemoresistance is reversible. a, Schematic of PDAC organoid expansion protocol for testing reversibility of stiffness-mediated chemoresistance. **b**,**c**, Summary of gemcitabine IC_{50} values for PDAC organoids expanded within HELP Low or HELP High matrices according to the protocol in **a**. PDAC cells were treated with gemcitabine throughout log-phase single-cell expansion (**b**) or following multicellular organoid formation (**c**) for six and three days, respectively. Each data point represents the mean ± 95% confidence interval ($N = 4$ independent experimental replicate hydrogels). Statistical analysis comparing IC_{50} values at passage 7 for all samples was performed using an ordinary one-way ANOVA with Tukey multiple comparisons correction (***$P < 0.001$, ****$P < 0.0001$; solid line compares non-switched HELP matrices, and dashed line compares switched HELP matrices). **d**,**e**, Single-cell-level (**d**) and organoid-level (**e**) gemcitabine dose–response curves for PDAC organoids expanded within HELP Low or HELP High for seven passages without (left) or with (right) a switch to the opposite matrix stiffness at passage 4. Each data point represents the mean ± s.e.m. ($N = 4$ independent experimental replicate hydrogels, solid centre line is nonlinear least squares regression of data, shaded region represents 95% confidence bands of nonlinear fit and data are normalized to positive controls (DMSO for single cells, 3,333 nM gemcitabine for organoids)). **f**, Quantification of mRNA-level *CD44* and *ABCG2* expression in PDAC organoids expanded within HELP Low or HELP High for seven passages, with or without a switch to the opposite matrix stiffness at passage 4 ($N = 4$ independent experimental replicate hydrogels, mean ± 95% confidence interval, ordinary one-way ANOVA with Tukey multiple comparisons correction, *$P < 0.05$; unlabelled comparisons are not significantly different). All data are normalized to *GAPDH* gene expression and respective marker expression in HELP Low at passage 7. **g**, Illustration summarizing mechanism of stiffness-mediated chemoresistance in this PDAC organoid model.

IC_{50} value decreased across both matrices compared to HELP matrices with RGD (Extended Data Fig. 3e,f). These results reveal that RGD signalling was not necessary for organoid expansion nor the establishment of increased chemoresistance in high-stiffness matrices, suggesting that RGD–integrin interactions are not the primary mechanism of stiffness-mediated PDAC chemoresistance.

To explore the effect of HA on PDAC organoids in our model, we modified our HELP matrix by replacing HA with an inert eight-arm polyethylene glycol (PEG) polymer to fabricate matrices we term ELP-PEG that are stiffness-matched to HELP Low and High (Fig. 4a,b and Supplementary Fig. 29). We found that PDAC organoids expanded robustly over four passages in ELP-PEG Low and High matrices despite the removal of HA (Fig. 4c and Supplementary Fig. 27b).

Interestingly, upregulation of *ABCG2* was lost in PDAC organoids expanded within ELP-PEG High compared to the ELP-PEG Low matrices following four passages (Fig. 4d). In agreement with this result, the stiffness-mediated chemoresistant phenotype was lost within ELP-PEG High compared to the ELP-PEG Low matrices, unlike the increased chemoresistance measured in HELP High matrices with HA (Fig. 4e,f). Taken together, these data suggest that HA signalling plays a substantial mechanistic role in PDAC chemoresistance via ABCG2 upregulation in our model.

HA–CD44 signalling mediates PDAC organoid chemoresistance

HA-mediated CD44 signalling has been linked to altered drug response in other cancer types[48]. To explore the hypothesis that HA–CD44 interactions promote chemoresistance in our model, we expanded PDAC organoids within HELP Low or HELP High and measured changes in CD44 expression. PDAC organoids from all three patient lines cultured in HELP High matrices showed increased mRNA expression of *CD44*, compared to HELP Low (Fig. 5a and Supplementary Fig. 17). Protein-level CD44 is similarly upregulated in organoids grown within HELP High compared to HELP Low (Fig. 5b,c). To functionally test the role of CD44, we knocked out the *CD44* gene via CRISPR/Cas9 in our patient-derived PDAC organoids (Fig. 5d,e and Supplementary Fig. 30a,b). CD44-negative cells were sorted, encapsulated in HELP Low and High matrices and expanded for four passages prior to gemcitabine treatment, alongside a wild-type control. We found that *CD44* knock-out (KO) PDAC organoids expanded robustly with similar growth rates between HELP Low and HELP High over four passages (Fig. 5f). As expected, *CD44* KO organoids have a significantly reduced expression of *CD44* in both the HELP Low and HELP High matrices (Fig. 5g). Importantly, we also show that *CD44* KO organoids cultured in HELP High matrices have significantly reduced *ABCG2* expression compared to wild-type organoids, while *ABCG2* expression in HELP Low matrices remains low for both wild-type and KO organoids (Fig. 5g). Moreover, *CD44* KO PDAC organoids within HELP High did not show an increase in resistance to gemcitabine treatment compared to HELP Low (Fig. 5h,i), unlike the wild-type control. Similarly, *CD44* KO organoids cultured in both HELP Low and HELP High showed increased chemosensitivity to paclitaxel (Supplementary Fig. 30c,d). Notably, both gemcitabine and paclitaxel sensitivity have been shown to be regulated through the ABCG2 efflux pump axis[37,49], further highlighting the connection between HA-mediated CD44 signalling and ABCG2 activity in the establishment of stiffness-based chemoresistance in our model.

Stiffness-mediated PDAC chemoresistance is reversible

Recent work has shown that the degradation of HA in the PDAC tumour microenvironment can improve survival in mouse models, with the hypothesis that it leads to increased drug delivery to the tumour[9]. Here we showed that PDAC organoids can dynamically alter their phenotype and drug sensitivity in response to HA-mediated CD44 interactions in a high-stiffness matrix, even when drug transport through high- and low-stiffness matrices is similar, leading us to hypothesize that reversing matrix stiffness may re-sensitize PDAC organoids to gemcitabine treatment.

To test this hypothesis, we expanded PDAC organoids in HELP Low or HELP High for a total of seven passages and performed drug treatment on a terminal subset of cells at passages one, four and seven. On the fourth passage, a subset of cells from each matrix were switched to the opposite stiffness matrix for the remaining three passages (Fig. 6a). Interestingly, in the passage immediately following the switch from one matrix to another, PDAC single cells and organoids retained short-term mechanical memory of their initial matrix stiffness (Fig. 6b,c and Supplementary Fig. 31). For example, despite being cultured within a HELP Low matrix after the switch at passage 4, PDAC organoids exhibited a similar gemcitabine IC_{50} value as organoids continuously maintained within HELP High. However, this mechanical memory was lost following an additional three passages within the opposite stiffness matrix (Fig. 6b–e). Overexpression of *CD44* and *ABCG2* was also reversible following several passages within the opposite stiffness matrix (Fig. 6f).

Outlook

Our data highlight how tunable engineered matrices can be leveraged to uncover the mechanistic roles of the ECM in driving human cancer organoid phenotype and drug response (Fig. 6g). These results suggest that the treatment of PDAC tumours with mechanotherapeutics that target matrix stiffness and/or cell–ECM interactions, such as HA–CD44 interactions, in combination with anticancer agents may improve tumour drug sensitivity and lead to improved patient outcomes. Notably, several mechanotherapeutics targeting cell–ECM signalling pathways are currently being explored in pancreatic cancer[50], highlighting the importance of considering the influence of ECM signalling when developing anticancer treatments. Additionally, this report identifies the extreme plasticity of drug efflux pump expression in response to a blocking agent and it suggests a potential mechanism for why efflux pump inhibitors have been ineffective in sensitizing tumours in the clinic[35]. Future strategies for sensitizing chemoresistant PDAC tumours may require combination therapies that target the source of altered transporter expression, such as the ECM properties identified here.

Online content

Any methods, additional references, Nature Portfolio reporting summaries, source data, extended data, supplementary information, acknowledgements, peer review information; details of author contributions and competing interests; and statements of data and code availability are available at https://doi.org/10.1038/s41563-024-01908-x.

References

1. Kleeff, J. et al. Pancreatic cancer. *Nat. Rev. Dis. Primers* **2**, 16022 (2016).
2. Siegel, R. L., Miller, K. D. & Jemal, A. Cancer statistics, 2015. *CA Cancer J. Clin.* **65**, 5–29 (2015).
3. Amrutkar, M. & Gladhaug, I. P. Pancreatic cancer chemoresistance to gemcitabine. *Cancers* **9**, 157 (2017).
4. Burris, H. A. et al. Improvements in survival and clinical benefit with gemcitabine as first-line therapy for patients with advanced pancreas cancer: a randomized trial. *J. Clin. Oncol.* **15**, 2403–2413 (1997).
5. Rahib, L., Fleshman, J. M., Matrisian, L. M. & Berlin, J. D. Evaluation of pancreatic cancer clinical trials and benchmarks for clinically meaningful future trials: a systematic review. *JAMA Oncol.* **2**, 1209–1216 (2016).
6. Hosein, A. N., Brekken, R. A. & Maitra, A. Pancreatic cancer stroma: an update on therapeutic targeting strategies. *Nat. Rev. Gastroenterol. Hepatol.* **17**, 487–505 (2020).
7. Feig, C. et al. The pancreas cancer microenvironment. *Clin. Cancer Res.* **18**, 4266–4276 (2012).

8. Tian, C. et al. Proteomic analyses of ECM during pancreatic ductal adenocarcinoma progression reveal different contributions by tumor and stromal cells. *Proc. Natl Acad. Sci. USA* **116**, 19609–19618 (2019).
9. Provenzano, P. P. et al. Enzymatic targeting of the stroma ablates physical barriers to treatment of pancreatic ductal adenocarcinoma. *Cancer Cell* **21**, 418–429 (2012).
10. Olive, K. P. et al. Inhibition of hedgehog signaling enhances delivery of chemotherapy in a mouse model of pancreatic cancer. *Science* **324**, 1457–1461 (2009).
11. Hakim, N., Patel, R., Devoe, C. & Saif, M. W. Why HALO 301 failed and implications for treatment of pancreatic cancer. *Pancreas Open J.* **3**, e1–e4 (2019).
12. Catenacci, D. V. T. et al. Randomized phase Ib/II study of gemcitabine plus placebo or vismodegib, a hedgehog pathway inhibitor, in patients with metastatic pancreatic cancer. *J. Clin. Oncol.* **33**, 4284–4292 (2015).
13. Henke, E., Nandigama, R. & Ergün, S. Extracellular matrix in the tumor microenvironment and its impact on cancer therapy. *Front. Mol. Biosci.* **6**, 160 (2020).
14. Paszek, M. J. et al. Tensional homeostasis and the malignant phenotype. *Cancer Cell* **8**, 241–254 (2005).
15. Chaudhuri, O. et al. Extracellular matrix stiffness and composition jointly regulate the induction of malignant phenotypes in mammary epithelium. *Nat. Mater.* **13**, 970–978 (2014).
16. LeSavage, B. L., Suhar, R. A., Broguiere, N., Lutolf, M. P. & Heilshorn, S. C. Next-generation cancer organoids. *Nat. Mater.* **21**, 143–159 (2022).
17. Drost, J. & Clevers, H. Organoids in cancer research. *Nat. Rev. Cancer* **18**, 407–418 (2018).
18. Boj, S. F. et al. Organoid models of human and mouse ductal pancreatic cancer. *Cell* **160**, 324–338 (2015).
19. Tiriac, H. et al. Organoid profiling identifies common responders to chemotherapy in pancreatic cancer. *Cancer Discov.* **8**, 1112–1129 (2018).
20. Hughes, C. S., Postovit, L. M. & Lajoie, G. A. Matrigel: a complex protein mixture required for optimal growth of cell culture. *Proteomics* **10**, 1886–1890 (2010).
21. Gjorevski, N. et al. Designer matrices for intestinal stem cell and organoid culture. *Nature* **539**, 560–564 (2016).
22. Hunt, D. R. et al. Engineered matrices enable the culture of human patient-derived intestinal organoids. *Adv. Sci.* **8**, 2004705 (2021).
23. Hernandez-Gordillo, V. et al. Fully synthetic matrices for in vitro culture of primary human intestinal enteroids and endometrial organoids. *Biomaterials* **254**, 120125 (2020).
24. Below, C. R. et al. A microenvironment-inspired synthetic three-dimensional model for pancreatic ductal adenocarcinoma organoids. *Nat. Mater.* **21**, 110–119 (2022).
25. Xiao, W. et al. Matrix stiffness mediates pancreatic cancer chemoresistance through induction of exosome hypersecretion in a cancer associated fibroblasts-tumor organoid biomimetic model. *Matrix Biol. Plus* **14**, 100111 (2022).
26. Tang, Z. et al. GEPIA: a web server for cancer and normal gene expression profiling and interactive analyses. *Nucleic Acids Res.* **45**, W98–W102 (2017).
27. LeSavage, B. L., Suhar, N. A., Madl, C. M. & Heilshorn, S. C. Production of elastin-like protein hydrogels for encapsulation and immunostaining of cells in 3D. *J. Vis. Exp.* **135**, e57739 (2018).
28. Connor, A. A. & Gallinger, S. Pancreatic cancer evolution and heterogeneity: integrating omics and clinical data. *Nat. Rev. Cancer* **22**, 131–142 (2021).
29. Roerink, S. F. et al. Intra-tumour diversification in colorectal cancer at the single-cell level. *Nature* **556**, 437–462 (2018).
30. Krieger, T. G. et al. Single-cell analysis of patient-derived PDAC organoids reveals cell state heterogeneity and a conserved developmental hierarchy. *Nat. Commun.* **12**, 5826 (2021).
31. Karlsson, K. et al. Deterministic evolution and stringent selection during preneoplasia. *Nature* **618**, 383–393 (2023).
32. Dean, M., Fojo, T. & Bates, S. Tumour stem cells and drug resistance. *Nat. Rev. Cancer* **5**, 275–284 (2005).
33. Fletcher, J. I., Williams, R. T., Henderson, M. J., Norris, M. D. & Haber, M. ABC transporters as mediators of drug resistance and contributors to cancer cell biology. *Drug Resist. Updates* **26**, 1–9 (2016).
34. Marzac, C. et al. ATP binding cassette transporters associated with chemoresistance: transcriptional profiling in extreme cohorts and their prognostic impact in a cohort of 281 acute myeloid leukemia patients. *Haematologica* **96**, 1293–1301 (2011).
35. Robey, R. W. et al. Revisiting the role of ABC transporters in multidrug-resistant cancer. *Nat. Rev. Cancer* **18**, 452–464 (2018).
36. Adamska, A. & Falasca, M. ATP-binding cassette transporters in progression and clinical outcome of pancreatic cancer: what is the way forward? *World J. Gastroenterol.* **24**, 3222–3238 (2018).
37. De Wolf, C. et al. Contribution of the drug transporter ABCG2 (breast cancer resistance protein) to resistance against anticancer nucleosides. *Mol. Cancer Ther.* **7**, 3092–3102 (2008).
38. Rudin, D., Li, L., Niu, N., Kalari, R. K. & Gilbert, A. J. Gemcitabine cytotoxicity: interaction of efflux and deamination. *J. Drug Metab. Toxicol.* **2**, 1000107 (2011).
39. Zhou, J. et al. Persistence of side population cells with high drug efflux capacity in pancreatic cancer. *World J. Gastroenterol.* **14**, 925–930 (2008).
40. Zhang, Z., Wang, J., Shen, B., Peng, C. & Zheng, M. The ABCC4 gene is a promising target for pancreatic cancer therapy. *Gene* **491**, 194–199 (2012).
41. Hsu, M. C. et al. Protein arginine methyltransferase 3 enhances chemoresistance in pancreatic cancer by methylating hnRNPA1 to increase ABCG2 expression. *Cancers* **11**, 8 (2019).
42. Golebiewska, A., Brons, N. H. C., Bjerkvig, R. & Niclou, S. P. Critical appraisal of the side population assay in stem cell and cancer stem cell research. *Cell Stem Cell* **8**, 136–147 (2011).
43. Zhou, S. et al. The ABC transporter Bcrp1/ABCG2 is expressed in a wide variety of stem cells and is a molecular determinant of the side-population phenotype. *Nat. Med.* **7**, 1028–1034 (2001).
44. Toyoda, Y., Takada, T. & Suzuki, H. Inhibitors of human ABCG2: from technical background to recent updates with clinical implications. *Front. Pharmacol.* **10**, 208 (2019).
45. Kim, Y. & Kumar, S. CD44-mediated adhesion to hyaluronic acid contributes to mechanosensing and invasive motility. *Mol. Cancer Res.* **12**, 1416–1429 (2014).
46. Geiger, B., Spatz, J. P. & Bershadsky, A. D. Environmental sensing through focal adhesions. *Nat. Rev. Mol. Cell Biol.* **10**, 21–33 (2009).
47. Nieberler, M. et al. Exploring the role of RGD-recognizing integrins in cancer. *Cancers* **9**, 116 (2017).
48. Chen, C., Zhao, S., Karnad, A. & Freeman, J. W. The biology and role of CD44 in cancer progression: therapeutic implications. *J. Hematol. Oncol.* **11**, 64 (2018).
49. Chung, W.-M. et al. Increase paclitaxel sensitivity to better suppress serous epithelial ovarian cancer via ablating androgen receptor/aryl hydrocarbon receptor-ABCG2 axis. *Cancers* **11**, 463 (2019).
50. Sheridan, C. Pancreatic cancer provides testbed for first mechanotherapeutics. *Nat. Biotechnol.* **37**, 829–831 (2019).

[1]Department of Bioengineering, Stanford University, Stanford, CA, USA. [2]Department of Chemical Engineering, Stanford University, Stanford, CA, USA. [3]Department of Materials Science and Engineering, Stanford University, Stanford, CA, USA. [4]Department of Medicine, Division of Oncology, Stanford University School of Medicine, Stanford, CA, USA. [5]Department of Genetics, Stanford University School of Medicine, Stanford, CA, USA. [6]Stanford Cancer Institute, Stanford University School of Medicine, Stanford, CA, USA. [7]Department of Medicine, Division of Hematology, Stanford University School of Medicine, Stanford, CA, USA. [8]Institute for Stem Cell Biology & Regenerative Medicine, Stanford University School of Medicine, Stanford, CA, USA. [9]Division of Infectious Diseases and Geographic Medicine, Department of Medicine, Stanford University School of Medicine, Stanford, CA, USA. [10]Department of Materials Science and Engineering, University of Pennsylvania, Philadelphia, PA, USA. [11]These authors contributed equally: Daiyao Zhang, Carla Huerta-López, Aidan E. Gilchrist. ✉e-mail: heilshorn@stanford.edu

Methods

Material synthesis and characterization

HELP, ELP-PEG and Cultrex matrix formation. For all experiments, HELP matrices were prepared by dissolving lyophilized HA and ELP components in a ×10 phosphate buffered saline solution (×10 PBS; 81 mM sodium phosphate dibasic, 19 mM sodium phosphate monobasic, 60 mM sodium chloride in Milli-Q water; pH 7.4) to a concentration double their final hydrogel concentration, allowing the formation of matrices upon a 1:1 mixture of stock HA–benzaldehyde and ELP–hydrazine solutions. Specifically, the appropriate volume of ×2 stock HA solution was added to the corresponding well/mould and an equal volume of ×2 stock ELP solution was pipetted directly onto the HA and immediately mixed using the same pipette tip. Both the HA and ELP solutions and the well plate containing the hydrogels was kept on ice during the mixing process. Following mixing, the matrices were immediately incubated at room temperature (r.t.) for 10 min (HELP Low and Medium) or 5 min (HELP High), followed by another incubation at 37 °C for 10 min (HELP Low and Medium) or 5 min (HELP High) to ensure complete gelation. Following gelation, matrices were submerged in PBS or cell culture medium depending on the application. ELP-PEG matrices were formed in the same way as HELP matrices, with a slight modification: HA–benzaldehyde was replaced with PEG–benzaldehyde and both the PEG and ELP components were dissolved in ×1 PBS. Cultrex solutions were stored at −80 °C and thawed on ice prior to use. The appropriate volume of Cultrex solution was pipetted into the corresponding well/mould without any dilution or modification and allowed to incubate at 37 °C for 10 min prior to submersion in PBS or cell culture medium depending on the application. The Supplementary Information contains detailed methods on the synthesis and characterization of all matrix components, and Supplementary Table 1 shows detailed final formulations for each matrix.

Hydrogel rheological characterization. Mechanical characterization was performed on all matrices using a stress-controlled AR-G2 rheometer (TA Instruments) and a cone-plate geometry (20 mm diameter, 1° cone angle, 28 µm gap between the geometry and stage). For HELP matrices, the ×2 HA and ×2 ELP stock solutions were combined and mixed on the centre of the rheometer stage using a pipette tip to form a 48 µl hydrogel. The geometry head was immediately lowered onto the sample, and the cross-linking reaction proceeded under 1% oscillatory strain and 1 rad s^{-1} angular frequency for 15 min at 23 °C, followed by a temperature ramp to 37 °C at 2 °C min^{-1} and another time sweep under 1% oscillatory strain and 1 rad s^{-1} angular frequency for 10 min at 37 °C. ELP-PEG matrices were formed on the rheometer stage, followed by an initial time sweep at 4 °C for 5 min, a time sweep at 23 °C for 10 min, a ramp to 37 °C at 2 °C min^{-1} and finally a time sweep at 37 °C for 10 min, all under 1% oscillatory strain and 1 rad s^{-1} angular frequency. For measuring the mechanics of Cultrex matrices, 48 µl of solution was added to the rheometer stage. The geometry head was immediately lowered onto the sample and the cross-linking reaction proceeded under 1% oscillatory strain and 1 rad s^{-1} angular frequency for 5 min at 23 °C followed by a time sweep under the same conditions for 5 min at 37 °C. Finally, for HELP, ELP-PEG and Cultrex matrices, a frequency sweep from 0.1 to 100 rad s^{-1} was performed under 1% oscillatory strain at 37 °C. The final shear modulus for all matrices was derived from the linear region of the frequency sweep at 1 rad s^{-1} angular frequency.

Human tissue analysis

Human tissue collection. Human, patient-derived primary PDAC, solid pseudopapillary neoplasm and normal adjacent pancreas tissue were obtained from the Stanford Tissue Bank from patients undergoing surgical resection at Stanford University Medical Center (SUMC). Procedures for the generation of human organoid lines from patient tissue samples were approved by the SUMC Institutional Review Board (IRB) and performed under protocol number 28908. All organoid lines used in this study were derived from treatment-naïve pancreatic tumours (Supplementary Table 3). Histological staining and mechanical testing of human tissue were deemed by the IRB to not involve human subjects as defined in US federal regulation 45 CFR 46.102(f) or 21 CFR 50.3(g), as the patient samples were de-identified prior to acquisition. All samples were confirmed to be tumour or normal adjacent by pathological assessment at SUMC. Written informed consent for research was obtained from donors prior to tissue acquisition.

Human tissue rheological characterization. Patient-derived normal and PDAC pancreas tissue was collected from surgical resection and placed in a mixture of advanced Dulbecco's Modified Eagle Medium and Ham's F-12 (ADMEM/F12; Gibco 12634010) supplemented with 10% foetal bovine serum (FBS; Sigma F0804) and 1% penicillin/streptomycin/glutamine (PSQ; Gibco 10378016). Mechanical measurements of tissue were collected between 1–4 h following surgical resection. Normal and PDAC tissues were cut using a biopsy punch and/or razor blade into 8-mm-diameter and 2–4-mm-thick sections. Mechanical characterization was performed using a stress-controlled AR-G2 rheometer (TA Instruments) using a parallel plate geometry (8 mm). The rheometer stage and geometry head were affixed with a thin section of sandpaper to prevent tissue slipping during measurements. To perform the measurements, the geometry head was lowered onto the tissue section, and once the normal force reached a value of 0.1–0.2 N, a frequency sweep was immediately performed. The final shear modulus was derived from the linear region of the frequency sweep from the average of five data points from 0.6–1.5 rad s^{-1} angular frequency. All measurements were collected at r.t.

Immunohistochemistry. Tissue sections were fixed in 4% paraformaldehyde (Electron Microscopy Sciences 15700) in PBS for 48 h at 4 °C, washed with PBS (3 × 15 min), paraffin embedded using step-wise dehydration, sectioned (~5 µm) and affixed to histology slides. Slides were then deparaffinized by two washes in fresh xylene (5 min each), followed by two washes in 100% ethanol (5 min each), one wash in 95% ethanol (1 min) and one wash in 70% ethanol (1 min) and were finally submerged in r.t. Milli-Q water. Heat-induced antigen retrieval was performed via a steamer for 30 min while slides were submerged in epitope retrieval solution (IHC World IW-1100). Next, slides were allowed to cool for 20 min before using a hydrophobic pen to isolate the tissue section of interest. Samples were permeabilized with 0.1% Triton X-100 (Thermo Fisher A16046) in PBS (PBST; 2 × 15 min) and blocked with 10% goat serum (Gibco 16210-072) in PBST for 90 min, all at r.t. Primary antibodies were diluted in sterile-filtered 0.05% Triton X-100, 0.1% bovine serum albumin (BSA; Sigma A9418) and 0.1% Tween-20 (Thermo Fisher AAJ20605AP) in PBS and incubated with the samples overnight at 4 °C. The following day, the samples were washed with PBST (3 × 15 min) and incubated with corresponding fluorescently tagged secondary antibodies and 4′,6-diamidino-2-phenylindole (DAPI; 5 mg ml^{-1} stock, 1:2,000) in the same antibody dilution solution for 2 h, all at r.t. Samples were again washed with PBST (3 × 15 min) and mounted to number 1 glass cover-slips with ProLong Gold Antifade Reagent (Cell Signaling 9071) for 48 h at r.t. Stained samples were imaged using an epifluorescent microscope (Leica Microsystems, THUNDER Imager 3D Cell Culture) and brightness/contrast was adjusted equally across comparative samples using ImageJ (National Institutes of Health, v.2.1.0/1.53c). Supplementary Tables 4 and 5 contain information about primary and secondary antibodies and their dilutions.

Cell culture and analysis

PDAC organoid culture. PDAC organoids consisting of only epithelial cancer cells were derived from surgically resected patient tissue using previously established methods[51]. For all experiments, PDAC organoids were used between an overall passage of 6 and 15. Where indicated in the main text and figure captions, PDAC organoids were expanded

within Cultrex, HELP or ELP-PEG matrices for at least four consecutive passages prior to performing drug treatment or cell analysis. These passage counts refer to the passage count throughout that specific experiment and not the overall passage count of the PDAC organoids. Cultures of primary solid pseudopapillary neoplasm organoids were cultured using the same protocols as the PDAC organoid lines.

PDAC organoid culture within Engelbreth–Holm–Swarm matrices, specifically Cultrex Reduced Growth-Factor Basement Membrane Extract, Type 2 (Biotechne R&D Systems 353301002), served as maintenance cultures throughout this study. Organoids were expanded within 40 µl Cultrex hydrogels immobilized in a custom 7-mm-diameter silicone mould affixed to a glass cover slip within a 24-well plate as previously reported[27]. Organoids were passaged in Cultrex matrices every seven to ten days upon reaching confluency. To passage organoids, Cultrex hydrogels were first dissociated in 5 mM ethylenediaminetetraacetic acid (EDTA) on ice for 30–45 min and pelleted at 500*g* for 5 min. Cell pellets were resuspended in 1 ml TrypLE (2 × 3 min incubations at 37 °C, with a pipette mixing in between; Gibco 12604013) to dissociate organoids into a single-cell suspension. The solutions were quenched in 40% FBS in PBS, and cells were pelleted at 500*g* for 5 min prior to being resuspended in complete WENR medium (full formulation below) supplemented with 2.5 µM CHIR99021 (Cayman Chemical 13122) and 10 µM Y-27632 hydrochloride (Cayman Chemical 10005583; Nucleotide: Y27632), filtered through a 40 µm cell strainer and counted. The desired number of cells were then pelleted at 500*g* for 5 min and resuspended in fresh, ice-cold Cultrex solution at 700 cells µl^{-1}. Cultrex hydrogels were formed as described above before adding 0.7 ml of fresh, prewarmed complete WENR medium supplemented with 2.5 µM CHIR99021 and 10 µM Y-27632 to each well of a 24-well plate containing one 40 µl hydrogel. After three days, the medium was changed to complete WENR medium without supplements, and the medium was changed every two days thereafter. Organoids were cultured at 37 °C in a humidified incubator with 5% CO_2. PDAC organoids were regularly tested for mycoplasma contamination using a MycoAlert Mycoplasma Detection Kit (Lonza LT07-318) and a Lucetta Single Tube Luminometer (Lonza AAL-1001).

To form cell-laden HELP matrices, PDAC organoids were released from Cultrex hydrogels and dissociated into a single-cell suspension as described above. The desired number of cells for the given experiment were pelleted at 500*g* for 5 min and resuspended in a ×2 stock solution of ELP–hydrazine. HELP matrix formation with cells was performed as described above before adding 0.7 ml of fresh, prewarmed complete WENR medium supplemented with 2.5 µM CHIR99021 and 10 µM Y-27632 to each well of a 24-well plate containing one 40 µl hydrogel. After three days, the medium was changed to complete WENR medium without supplements, and the medium was changed every two to three days thereafter. If relevant to the given experiment, PDAC organoids were passaged in HELP matrices every 10–14 days upon reaching confluency. To passage organoids, HELP matrices were removed from the silicone moulds using a spatula and transferred to a 1.5 ml Eppendorf tube (epi-tube) containing an equal volume of HELP dissociation solution (PBS supplemented with 200 U ml^{-1} elastase (GoldBio E-240-1), 2,000 U ml^{-1} hyaluronidase (Sigma H3506), 3 mM EDTA and 20% v/v complete WENR medium). This mixture was incubated for 45 min at 37 °C and pipette mixed every 15 min to aid in hydrogel degradation. Samples were then pelleted, dissociated with TrypLE, resuspended in media and counted as described above for passaging organoids in Cultrex matrices. PDAC organoids were encapsulated in HELP matrices as single cells at 1,000 cells µl^{-1} or 750 cells µl^{-1} for routine passaging or for all comparative experiments, respectively.

The formation of cell-laden ELP-PEG matrices was the same as HELP matrices, with some slight alterations as described above in Methods section on matrix formation. To passage in ELP-PEG matrices, ELP-PEG hydrogels were collected from culture into a 1.5 ml epi-tube containing an equal volume of ELP-PEG dissociation solution (PBS supplemented with 400 U ml^{-1} elastase (GoldBio E-240-1), 3 mM EDTA and 20% v/v complete WENR medium) and incubated for 1 h at 37 °C with regular pipette mixing. The remaining steps to fully release the organoids from ELP-PEG matrices were identical to the HELP protocols presented above.

PDAC organoid media generation. Complete WENR medium used throughout these studies was composed of a 1:1 mixture of ADMEM/F12 base medium and LWRN-cell-conditioned medium (LWRN, American Type Culture Collection (ATCC) CRL-3276). To prepare the conditioned medium, LWRN cells were expanded for one to two days in T150 tissue culture flasks in maintenance medium (DMEM (Gibco 11960044) supplemented with 10% FBS and 1% PSQ). Upon reaching 80% confluence, cells were split 1:4. After one day, the growth medium was supplemented with 500 µg ml^{-1} G418 (Gibco 10131-035) and hygromycin B (Invitrogen 10687010) selection factors to ensure selection of stable clones containing the expression vectors for Wnt3A, R-spondin 3 and Noggin. Cells were passaged twice more in selection medium and split into several T150 flasks with maintenance medium. Upon reaching 80% confluency, cells were washed with PBS, and 25 ml of collection medium (ADMEM/F12 supplemented with 10% FBS and 1% PSQ) was added to the cells. After 24 h, conditioned medium was collected from all flasks, spun down to remove cell debris (2,000*g* for 5 min), filtered and combined into a single container. Fresh collection medium was added to each flask and the conditioned medium was collected in the same manner for up to four collections. To make the complete WENR medium, LWRN-conditioned media was combined 1:1 with ADMEM/F12 and supplemented with 1 mM HEPES buffer (Gibco 15630106), 1% GlutaMax (Invitrogen 35050061), 10 mM nicotinamide (Sigma N0636), 1 mM *N*-acetylcysteine (Sigma A9165), 2% B-27 Supplement without vitamin A (Invitrogen 12587010), 0.5 µM A83-01 (Cayman Chemical 9001799), 1% PSQ, 10 nM Gastrin I (Cayman Chemical 24457), 10 µM SB-202190 (Cayman Chemical 10010399), 50 ng ml^{-1} recombinant human epidermal growth factor (EGF; Peprotech AF-100-15) and 100 µg ml^{-1} Normocin (Invivogen ANT-NR-1).

Bright-field imaging and organoid diameter quantification. PDAC organoids previously expanded in Cultrex matrices were dissociated into a single-cell suspension and encapsulated in 20 µl Cultrex or HELP matrices at a density of 750 cells µl^{-1} as above. Organoids were imaged every other day from day 1 until reaching confluence (day 15, Cultrex; day 17, HELP) via phase contrast (Leica Microsystems, THUNDER Imager 3D Cell Culture) using a ×10 objective. At least eight non-overlapping images were taken of $N = 3$ independent replicate hydrogels for each matrix type. Organoid diameter was measured using ImageJ (NIH, v.2.1.0/1.53c).

Chemotherapy treatment and sensitivity measurement via cleaved caspase 3. To assess PDAC organoid gemcitabine sensitivity through activation of caspase 3, organoids were encapsulated as single cells within the indicated matrices at an initial density of 750 cells µl^{-1}. PDAC organoids were grown to an average diameter of ~75 µm prior to being treated with either 0.1% DMSO (control; Sigma G6423) or 100 nM gemcitabine hydrochloride supplemented in complete WENR medium for three days. Within the three days, one medium change with fresh DMSO or gemcitabine was performed 24 h after the initial drug treatment. Following the drug treatment, organoids were fixed and stained for cleaved caspase 3 expression following the whole mount immunofluorescence protocol below. DAPI and phalloidin were used to stain nuclei and F-actin, respectively. Stained samples for each matrix were imaged using a confocal microscope (Leica SPE) and a ×20 objective for a 550 µm × 550 µm field of view; care was taken to image samples under the same imaging parameters. Some five to eight non-overlapping *z* stacks (*z* range, 100–300 µm; image intervals, 10 µm) were taken per hydrogel per condition. Three biological replicate hydrogels were

analysed for each condition, yielding a range of 20–24 total *z* stacks each containing several organoids. For each *z* stack containing several organoids, the total cleaved caspase 3 area was divided by the total nucleus count to calculate the area of cleaved caspase 3 signal per nucleus. Quantification of cleaved caspase 3 signal was performed using ImageJ (NIH, v.2.1.0/1.53c) and all images were blinded to the researcher during analysis. The same analysis pipeline using identical tool/plugin parameters was performed on all samples in the experiment. Briefly, for each image, Li's minimum cross entropy thresholding method was performed to create a binary mask of positive cleaved caspase 3 signal and the 'measure' function was used to find the total cleaved caspase 3 area in micrometres squared. For the same image, the 'find maxima' and 'analyze particles' tools were used to count the number of nuclei. The cleaved caspase 3 signals for gemcitabine-treated and DMSO-treated samples were individually normalized to the DMSO control for each matrix.

Chemotherapy treatment and sensitivity measurement via Cell Titer Glo and CytoTox Glo. For generation of IC_{50} curves, PDAC organoids from all four pancreatic cancer lines (three PDAC and one primary solid pseudopapillary neoplasm) were cultured and treated with gemcitabine at one of two stages of organoid culture: (1) drug treatment throughout the log-phase expansion of single cells into multicellular organoids or (2) drug treatment upon formation of ~75-µm-diameter multicellular organoids. These two drug treatment protocols were run in parallel to study the effect of timing of drug treatment on the organoids during their growth, as well as to validate the results using two distinct assay read-outs (Cell Titer Glo versus CytoTox Glo; more detail is below). In addition, PDAC patient number 1 was treated with paclitaxel or with FOI using the single-cell drug treatment protocol. FOI is a combination of chemotherapy drugs (fluorouracil, oxaliplatin, irinotecan) added in molar concentration ratios 1:1:0.001, respectively. The reported concentrations for FOI are the concentrations of fluorouracil and oxaliplatin. For all these experiments, Cultrex, HELP and ELP-PEG matrices (25 µl) were prepared within a clear-bottom, half-area, black 96-well plate (Greiner Bio-One 675090) following the procedures listed above. For each experiment, a total of three to five replicate hydrogels were cast for each drug concentration within a given condition.

For organoid drug treatment, PDAC organoids were seeded as single cells in their respective matrices at a density of 750 cells μl^{-1} and were grown to an average diameter of ~75 µm prior to being treated with DMSO (0.1%) and 3, 33, 66, 100, 200, 333, 1,000 or 3,333 nM gemcitabine for three days. Within the three days, one media change with fresh DMSO or gemcitabine was performed 24 h after the initial drug treatment. Following drug treatment, cell toxicity was measured for each sample using a CytoTox Glo Assay (Promega G9290) and a LUMIstar Omega microplate luminometer (BMG Labtech). Toxicity measurements were normalized to DMSO (that is, 0) and 3,333 nM gemcitabine (that is, 1). A least squares nonlinear regression method ('[Inhibitor] vs. response -- Variable slope' with four parameters) was used to calculate the best fit and IC_{50} value for each experimental group using GraphPad Prism software (v.9.3.1).

For single-cell drug treatment, PDAC organoids were seeded as single cells in their respective matrices at a density of 750 cells μl^{-1} and were grown for two days (Cultrex) or four days (HELP and ELP-PEG) prior to being treated with DMSO (0.1%), 3, 10, 33, 66, 100, 200, 333 or 3,333 nM gemcitabine; or DMSO (0.1%), 0.5, 1, 2.5, 5, 10, 25, 50, 100 or 500 nM paclitaxel; or DMSO (0.1%), 0.01, 0.05, 0.1, 0.25, 0.5, 1, 2.5, 5 or 10 µM FOI for six days. Media supplemented with DMSO or drug was replaced every other day. Following drug treatment, cell viability was measured for each sample using a Cell Titer Glo 3D Assay (Promega G9681) and a LUMIstar Omega microplate luminometer (BMG Labtech). Within an experiment, viability measurements were normalized to DMSO or the lowest drug concentration (that is, 1). The best fit and IC_{50} values were calculated as described above.

Drug efflux pump inhibitor treatment. To test the role of ABCG2 inhibition on PDAC organoid gemcitabine sensitivity, PDAC organoids were encapsulated in Cultrex or HELP matrices and treated with drug/inhibitor following the 'single-cell' and 'organoid' treatment protocols described above. Specifically, for single-cell treatment, cells were treated with either 0.2% DMSO, 33/66 nM gemcitabine or 33/66 nM gemcitabine + 20 µM Ko143 (Cayman Chemical 15215). For organoid treatment, organoids were treated with either 0.2% DMSO, 100 nM gemcitabine, 100 nM gemcitabine + 20 µM Ko143 or 3,333 nM gemcitabine (positive control). PDAC viability upon treatment of 20 µM Ko143 alone was measured following the single-cell treatment protocol. The same protocols were followed for treatment with 50 µM verapamil (Sigma 1711202).

Quantitative polymerase chain reaction. For qPCR analysis, PDAC organoids cultured within 40 µl Cultrex, HELP or ELP-PEG matrices were dissociated for 20–30 min at 37 °C in 40 µl of HELP or ELP-PEG dissociation solution. Cultrex matrices were dissociated in HELP dissociation solution to expose all cells to the same treatment. Next, the samples were immediately resuspended in 500 µl of TRIzol reagent (Invitrogen 15596018) and frozen at −80 °C until use. The mRNA was purified from lysates using a phenol–chloroform extraction. First, samples were disrupted via probe sonication (Heilscher UP50H, 50% amplitude (25 W), 30 kHz frequency, 0.5 cycle), transferred to a phase lock gel (Quantabio 5PRIME 2302830) and supplemented with 100 µl chloroform (Sigma CX1055). Samples were then centrifuged at 15,300*g* at 4 °C for 15 min and the top, aqueous phase was transferred to a clean 1.5 ml epi-tube. Samples were precipitated with one wash of isopropyl alcohol followed by two washes of 70% ethanol with centrifugation steps between each wash (18,500*g* at 4 °C for 10 min). After decanting the final ethanol wash, samples were dried and resuspended in 15–30 µl of nuclease-free water. The mRNA concentrations were measured via NanoDrop (Thermo Scientific) and a consistent amount of mRNA across all samples (100–1,000 ng) was reverse transcribed using a High-Capacity cDNA Reverse Transcription Kit (Applied Biosystems 4368814). The qPCR was performed on 6.6 µl of diluted complementary DNA (cDNA) per gene target mixed with 0.9 µl of 5 µM forward and reverse primer pair solution and 7.5 µl of Fast SYBR Green Master Mix (Applied Biosystems 4385612). Samples were run on a StepOnePlus Real Time PCR System (Applied Biosystems). Cycle threshold (CT) values were calculated using the StepOnePlus software (v.2.3) and normalized to *GAPDH* as a housekeeping gene (ΔCT). Integrin and ECM component expression data (Supplementary Fig. 28) are reported using both the ΔCT (Supplementary Fig. 28a) and ΔΔCT (Supplementary Fig. 28b) methods to enable a comparison of expression levels across markers of interest. All other datasets are presented as values normalized to Cultrex (ΔΔCT method). Statistical analysis was performed prior to transforming to a natural scale as ΔΔCT values approximate a normal distribution. The mRNA expression data throughout the paper is reported as a geometric mean with asymmetric 95% confidence intervals derived from the non-transformed data. Supplementary Table 6 contains information about qPCR primers. Melt curves were performed for all primers pairs.

Immunofluorescence imaging. PDAC organoids cultured within HELP and Cultrex matrices were prepared for immunostaining using two different methods: (1) paraffin embedding and sectioning or (2) whole mount in situ 3D staining and imaging.

For paraffin embedded samples, HELP and Cultrex matrices containing PDAC organoids were washed with 1 ml PBS and fixed with 1 ml 4% paraformaldehyde and 0.1% glutaraldehyde (Thermo Fisher BP25481) in PBS for 48 h at 4 °C. Samples were then washed with 200 mM glycine in PBS (1 × 15 min) to quench any remaining glutaraldehyde, followed by washes with PBS (2 × 10 min). Subsequent paraffin embedding, sectioning, staining and mounting were performed

as described above for human tissue sections. Stained samples were imaged using an epifluorescent microscope (Leica Microsystems, THUNDER Imager 3D Cell Culture), and care was taken to scale intensity values equally across all images when comparing protein expression across samples using ImageJ (NIH, v.2.1.0/1.53c). Supplementary Tables 4 and 5 contain information about primary and secondary antibodies and their dilutions.

For whole mount 3D samples, HELP and Cultrex matrices containing PDAC organoids were washed with 1 ml PBS and fixed with 1 ml 4% paraformaldehyde and 0.1% glutaraldehyde in PBS for 30 min at 37 °C. Samples were then washed with 200 mM glycine in PBS (1 × 15 min) to quench any remaining glutaraldehyde, followed by washes with PBS (2 × 10 min). Next, the samples were permeabilized with 1 ml PBST for 1 h at r.t. while rocking and subsequently blocked with 1 ml 10% goat serum in PBST for 4 h at r.t. Primary antibodies were diluted in sterile-filtered 0.05% Triton X-100, 0.1% BSA and 0.1% Tween-20 in PBS, and 400 µl of primary antibody solution was added to each sample to incubate overnight at 4 °C. The following day, the samples were washed with 1 ml PBST (3 × 15 min) at r.t. and incubated with 400 µl of the corresponding fluorescently tagged secondary antibodies, DAPI (5 mg ml^{-1} stock, 1:2,000) and/or tetramethylrhodamine (TRITC)–phalloidin (100 µg ml^{-1} in DMSO stock, 1:500) in the same antibody dilution solution overnight at 4 °C. Samples were again washed with PBST (3 × 15 min) and mounted to number 1 glass cover-slips with ProLong Gold Antifade Reagent for 48 h at r.t. Stained samples were imaged using a confocal microscope (Leica SPE), and care was taken to scale intensity values equally across all images using ImageJ (NIH, v.2.1.0/1.53c) when comparing protein expression across samples. Supplementary Tables 4 and 5 contain information about primary and secondary antibodies and their dilutions.

Organoid barcoding and analysis. Genetically barcoded PDAC organoids were generated as previously described[31]. For this work, genetically barcoded PDAC organoids were expanded within Cultrex, HELP Low or HELP High matrices for a total of three passages from the initial parent population established within Cultrex. For each passage, organoids were expanded in their respective matrices until reaching confluence, and organoids were released from the matrices and dissociated into a single-cell solution as described above (that is, Cultrex and HELP matrices were dissociated using the same dissociation solutions and protocols). One million cells were collected for DNA barcode sequencing from the initial parent population and between each passage from $N = 3$ independent, technical replicates from each matrix type. These samples were washed with PBS, pelleted and frozen at −80 °C until use. DNA extraction was performed using either a QIAamp DNA Micro Kit or DNeasy Blood and Tissue Kit (Qiagen 56304/69504) and double-stranded DNA (dsDNA) was measured using Qubit Fluorometer (Invitrogen Q33238) and Qubit dsDNA HS Assay Kit (Invitrogen Q32851).

Barcode sequencing and analysis was performed similarly to previous work[31]. Briefly, the barcode region was amplified by PCR using 2X KAPA Hifi PCR Master Mix (Roche Sequencing Solutions KK2601) with a minimum of 200 ng of DNA input per sample. The PCR product was purified using Ampure magnetic beads (Beckman Coulter A63881) and then subjected to a second PCR reaction where sequencing adaptors with sample specific indexes were added. The PCR products of all samples were then combined and purified using a Qiagen PCR purification kit. To remove primer dimers, the purified product was run on a 2% EX gel (Thermo Fischer G401002) and the 200 base-pair band was isolated and gel purified using a Qiaquick gel extraction kit (Qiagen 28706). The purified product was bioanalysed and confirmed for a 204 base-pair peak prior to sequencing with 150 base-pair paired-end reads on an Illumina MiSeq.

For extraction of cell barcodes from sequencing FASTQ files, only reads exactly matching the sequence around the 30 base-pair barcode were retained to ensure read quality. Then, reads from all samples were combined into a single file, and UMI-tools was used to merge similar barcode reads (that is, reads where the difference between barcodes was more likely to depend on sequencing and PCR errors, as compared to being a separate barcode). Each such group of combined barcodes was called a read group. Barcode reads for individual samples were then matched to the file containing all read groups, and associated barcode reads and counts for each read group were summed per sample. For each sample, the number of reads per barcode was normalized by the total read count to calculate the barcode frequency. To mitigate noise, a barcode frequency cut-off of 0.01% was applied to all samples, which removed <2.5% of reads for each replicate. For analysis of barcodes present at passage 3, a barcode was included only if it met the frequency cut-off in all three biological replicates for a given matrix. Data analysis was conducted using MATLAB (v.9.11.0.1769968). In Extended Data Fig. 1f, some barcodes may have average frequencies of <0.01% because the specific clone had an average frequency of >0.01% in at least one matrix type. In Supplementary Figs. 13 and 14, barcode frequencies at passage 3 within each matrix were normalized by their initial frequency in the parent population.

SP assay and cell cycle analysis. PDAC organoids expanded within Cultrex or HELP matrices were collected and dissociated into single cells as described above. Single cells were immediately resuspended in warm complete WENR medium supplemented with 5% FBS and 10 µM Y-27632 (Cayman Chemical 10005583) solubilized in water at a density of 10^6 cells ml^{-1}. Hoechst 33342 (Thermo Fisher H3570) was added to all conditions at a concentration of 5 µg ml^{-1}, and Ko143 (200 nM; Cayman Chemical 15215) or verapamil (50 µM; Sigma V4629) solubilized in water was added to inhibition samples. Ko143 was first solubilized in DMSO at 10 µM and then diluted in PBS to 4 µM before being added to the media at a final concentration of 200 nM. Samples were immediately moved to 37 °C for 2 h, with gentle mixing every 15 min to reduce cell settling. After treatment, cell pellets were collected (5 min, 500*g*) and resuspended in ice-cold flow buffer (PBS + 5% FBS) with 7-AAD viability dye (5:100; Thermo Fisher 00-6993-50) and immediately used for flow cytometry on a BD FACSymphony A5 analyser. The flow rate was kept to below 200 events per second, and a minimum of 50,000 live, single-cell events were recorded for each sample. The SP was detected using a 428/31 nm band-pass filter (Hoechst blue) and a 670/30 nm band-pass and 635 nm long-pass filter (Hoechst red); excitation was with a UV (305 nm) laser. Verapamil samples were used to confirm the gating strategy for the identification of the SP. DNA content for cell cycle analysis was detected using a 428/31 nm band-pass filter and excited with a UV (305 nm) laser. Cells in the S phase were identified as the region between G0/G1 and G2 peaks. All flow cytometry analysis was performed with FlowJo software (v.10.7.1). For sorting of the SP, G0/G1 and viable cells, collection was performed on a BD FACSymphony S6 sorter following the same protocol as above.

Flow cytometry. PDAC organoids expanded within Cultrex or HELP matrices were collected and dissociated into single cells as above. Single cells were immediately resuspended in ice-cold flow buffer (PBS + 5% FBS) with Fc receptor block (20:100; Thermo Fisher 14-9161-73). After 20 min, samples were stained for surface protein expression for 30 min on ice. Samples were washed in ice-cold flow buffer and pelleted (5 min, 500*g*). Samples were resuspended in flow buffer with 7-AAD viability dye (5:100; Thermo Fisher 00-6993-50) and immediately used for flow cytometry on a BD FACSymphony A5 instrument. A minimum of 50,000 live, single-cell events were recorded for each sample. Compensation was set using UltraComp eBeads Compensation Beads (Thermo Fisher 01-2222-41) and unstained cells. Fluorescence minus one controls were used to set gating strategies. All antibody stains were titrated prior to use to identify the optimal concentration for the separation of negative and positive populations. Supplementary Table 4 contains antibodies and dilutions. All flow cytometry analysis

was performed with FlowJo software (v.10.7.1). All values are reported as the median intensity of the live population.

***CD44* KO with CRISPR/Cas9.** PDAC organoids from patient number 1 were cultured in Cultrex matrices for eight days. Roughly 200,000 single cells were isolated as previously described and electroporated with 60 pmol single-guide RNA (UCGCUACAGCAUCUCUCGGA) targeting *CD44* exon 2 (IDT) and 30 pmol Alt-R S.p. Cas9 Nuclease V3 Cas9 (IDT 1081058) in 20 µl P3 buffer (Lonza V4XP-3032). Samples were electroporated using a 4D-Nucleofector X Unit (Lonza) and electroporation code CM-130. A wild-type (electroporation-only) control was run using all the same conditions in the absence of the sgRNA. Following electroporation, all samples were re-encapsulated in Cultrex matrices at 1,000 cells μl^{-1} for six days. Organoids were then sorted for the viable, CD44− population via FACS, and re-encapsulated in Cultrex matrices for eight days. Wild-type and *CD44* KO cells were then seeded as single cells into HELP Low and HELP High matrices and passaged four consecutive times prior to drug treatment and analysis, as previously described. A subset of sorted cells (~100,000) was collected for DNA extraction using the Fast Tissue/Tail PCR Genotyping Kit (EZ BioResearch G1001-100) and sent for genotyping. The ICE analysis tool from Synthego (https://ice.synthego.com/#/; v.3.0) was used to verify the cut site and estimate KO efficiency.

Other

Tumour versus normal RNA-seq analysis. Analysis of RNA-seq data was performed using a previously published GEPIA online tool[26] collecting data from TCGA and The Genotype Tissue Expression Project (GTEx). Specifically, the online GEPIA toolkit pulls its RNA-seq data from the University of California, Santa Cruz Xena project[52] and the University of California, Santa Cruz Toil RNAseq Recompute Compendium[53], which have recomputed the raw expression data from both the TCGA and GTEx datasets using a standard protocol to eliminate batch effects and issues arising from different sequencing methods. The pancreatic adenocarcinoma ('PAAD') dataset was used. The data were plotted on a log scale ($\log_2(\mathrm{TPM}+1)$) with a jitter size of 0.4. 'Match TCGA normal and GTEx data' was selected.

Statistical analysis. Statistical analyses for this study were performed using GraphPad Prism v.9.3.1 software. Details of specific statistical methods and *P* value results are included within the figure captions. For all studies, NS means not significant ($P > 0.05$), $^{*}P < 0.05$, $^{**}P < 0.01$, $^{***}P < 0.001$ and $^{****}P < 0.0001$.

Reporting summary

Further information on research design is available in the Nature Portfolio Reporting Summary linked to this article.

Data availability

All data needed to evaluate the conclusions in the paper are present in the paper and/or the Supplementary Information. Raw data related to this paper are uploaded to the Stanford Digital Repository, which can be accessed through the persistent URL (https://purl.stanford.edu/nw595bg6402) and the DOI (https://doi.org/10.25740/nw595bg6402). RNA-seq data from the TCGA and GTEx databases were accessed and plotted using the GEPIA online tool (http://gepia.cancer-pku.cn). Source data are provided with this paper.

References

51. Neal, J. T. et al. Organoid modeling of the tumor immune microenvironment. *Cell* **175**, 1972–1988.e16 (2018).
52. Goldman, M. J. et al. Visualizing and interpreting cancer genomics data via the Xena platform. *Nat. Biotechnol.* **38**, 675–678 (2020).
53. Vivian, J. et al. Toil enables reproducible, open source, big biomedical data analyses. *Nat. Biotechnol.* **35**, 314–316 (2017).

Acknowledgements

We thank T. Lozanoski, E. Rankin, S. Natarajan and J. Roth for insightful conversations and editing of the paper. We are grateful to the patients who donated tissue samples used for this research. We thank the Stanford Tissue Bank for their assistance in procuring patient tissue samples. We thank Z. Ma for help with barcode DNA sequencing. We thank P. Chu at the Stanford Human Pathology/Histology Service Center for assistance with tissue and organoid paraffin embedding and sectioning. B.L.L. acknowledges financial support from the Siebel Scholars Program and Stanford Bio-X Bowes Graduate Fellowship. D.Z. acknowledges financial support from the Stanford Graduate Fellowship and the National Science Foundation Graduate Research Fellowship Program. C.H.-L. acknowledges financial support from Fundación Alfonso Martín Escudero. B.A.K. acknowledges financial support from the Stanford Bio-X Bowes Graduate Fellowship. K. Karlsson acknowledges financial support from the Swedish Research Council (2018-00454). K.C.K. acknowledges financial support from the National Science Foundation Graduate Research Fellowship Program. M.S.H. acknowledges financial support from the National Institutes of Health F31 Pre-Doctoral Fellowship (NS132505), the Stanford ChEM-H O'Leary-Thiry Graduate Fellowship and the Gerald J. Lieberman Fellowship. This work was supported by funding from the National Institutes of Health (R01 EB027171 to S.C.H.; R01CA2515143, U01CA217851 and U54CA224081 to C.J.K.; U01CA217851 and DP1CA238296 to C.C.), Stand Up to Cancer and Cancer Research UK (C.J.K.), and the National Science Foundation (CBET 2033302 to S.C.H.). Flow cytometry data were collected on BD FACSymphony A5 in the Shared FACS Facility, obtained using a NIH S10 Shared Instrument Grant (1S10OD026831-01). Part of this work was performed at the Stanford Nano Shared Facilities (SNSF), supported by the National Science Foundation under award ECCS-2026822.

Author contributions

B.L.L., D.Z., C.H.-L., A.E.G., B.A.K., A.R.S. and S.C.H. designed the research. B.L.L., D.Z., C.H.-L., A.E.G., B.A.K., K. Karagyozova, K.C.K., M.S.H., C.L., G.K. and C.M.M. conducted experiments. B.L.L., D.Z., C.H.-L., A.E.G., K. Karlsson, C.L., G.K. and C.M.M. analysed data. K. Karlsson, A.R.S., C.C. and C.J.K. provided organoids and reagents. B.L.L., D.Z., C.H.-L. and A.E.G. wrote the paper. B.L.L., D.Z., C.H.-L., A.E.G., B.A.K., K. Karlsson, A.R.S., K. Karagyozova, K.C.K., M.S.H., C.L., G.K., C.M.M., P.L.B., C.C., C.J.K. and S.C.H. edited and approved the final paper.

Competing interests

S.C.H. has a patent application pending related to the hydrogel formulations used in this paper, as described in an international patent application PCT/US/2021/057925 with an international filing date of 3 November 2021. This application has been submitted to the U.S. Patent Office and published on 16 November 2023 as US 2023-0365940 A1, and this same application has entered the national phase in China (publication number 116829126), Singapore (application number 11202303493U), Europe (publication number 4240327), Japan (serial number 2023-526661), Canada (serial number 3,196,621), Israel (serial number 302453), South Korea (serial number 10-2023-7018686) and Australia (serial number 2021376143). The named inventors are S. Heilshorn, R. Suhar and D. Hunt, and the named applicant is the Board of Trustees of the Leland Stanford Junior University. C.C. is an advisor and holds equity in Grail, Ravel and Deepcell, and is an advisor to Genentech and NanoString. C.J.K. is an advisor and holds equity in Surrozen, Mozart and NextVivo. The other authors declare no competing interests.

Additional information

Extended data is available for this paper at https://doi.org/10.1038/s41563-024-01908-x.

Supplementary information The online version contains supplementary material available at https://doi.org/10.1038/s41563-024-01908-x.

Correspondence and requests for materials should be addressed to Sarah C. Heilshorn.

Peer review information *Nature Materials* thanks Toshiro Sato and the other, anonymous, reviewer(s) for their contribution to the peer review of this work.

https://doi.org/10.1038/s41563-024-01908-x

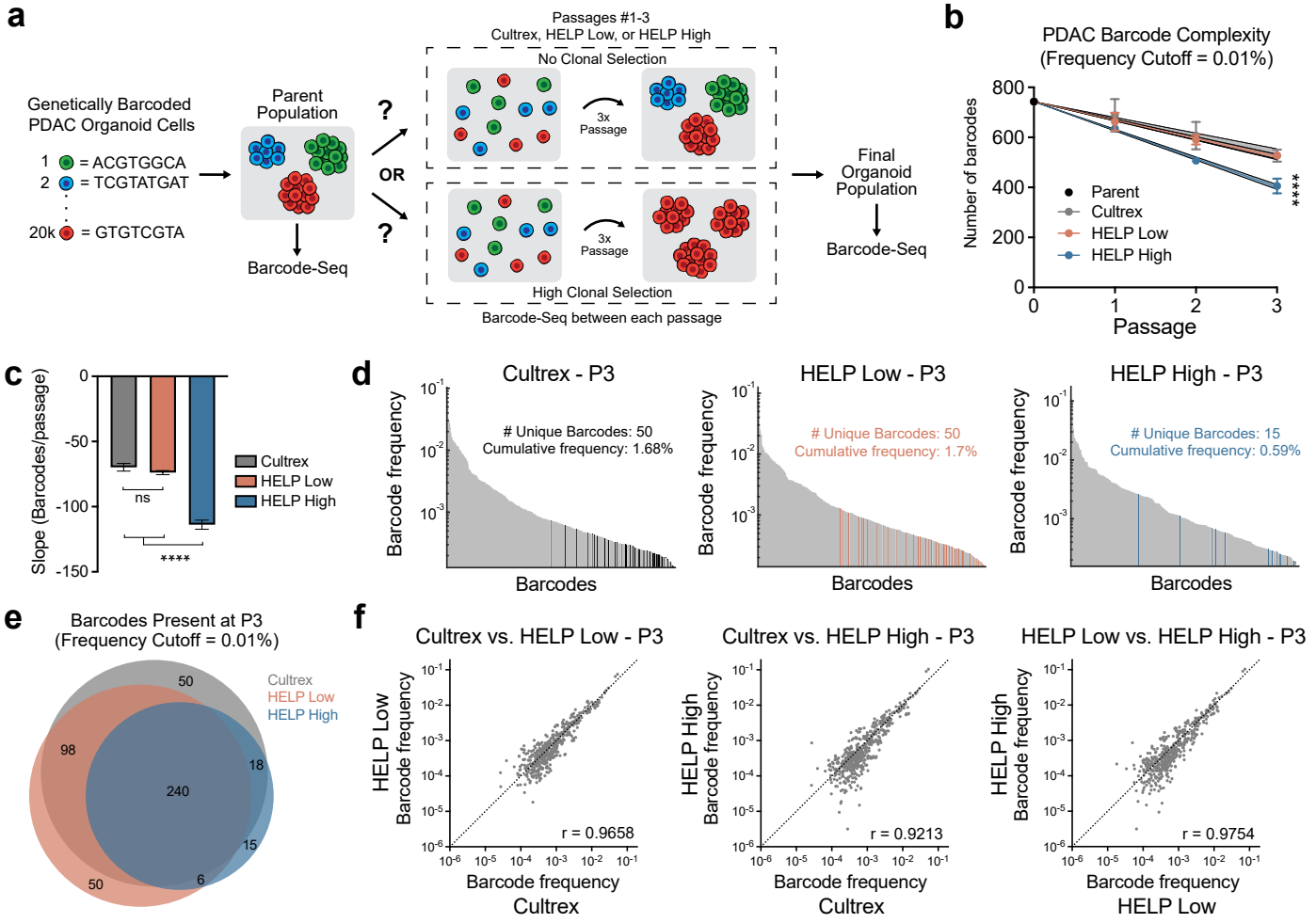

Extended Data Fig. 1 | Matrix stiffness mediates PDAC organoid clonal heterogeneity. a, Schematic summarizing the protocol and potential outcomes of genetically barcoded PDAC organoid expansion within Cultrex and HELP matrices. **b**, Number of barcodes present within PDAC organoid populations expanded within Cultrex and HELP matrices for one to three passages ($N = 3$ independent biological replicates per matrix type, mean ± 95% confidence interval, center line represents linear fit for each matrix over three passages, shaded region represents 95% confidence interval of linear fit). Statistical analysis was performed using an ordinary one-way ANOVA with Tukey multiple comparisons correction between data points at passage three (****$P < 0.0001$ for comparison between HELP High and Cultrex/HELP Low, comparison between HELP Low and Cultrex was not significantly different). The initial Parent population was the same for all matrices ($N = 1$). **c**, Slope of linear fit from **b** for each matrix ($N = 3$ independent biological replicates per matrix type, mean ± 95% confidence interval, ordinary one-way ANOVA with Tukey multiple comparisons correction, ****$P < 0.0001$, NS, not significant). **d**, Frequencies of barcodes present in the indicated matrix at passage three. Barcodes are listed in rank order and colored bars correspond to barcodes unique to only the indicated matrix. The number of these unique barcodes and their cumulative frequency are reported for each matrix. **e**, Venn diagram of barcodes at passage three across indicated matrices. **f**, Correlation plots comparing barcode frequencies across Cultrex and HELP at passage three. Pearson r values are reported for each pairing. Dashed line represents perfect correlation. In **d**-**f**, only barcodes with a frequency >0.01% across all three biological replicates at passage three were included.

https://doi.org/10.1038/s41563-024-01908-x

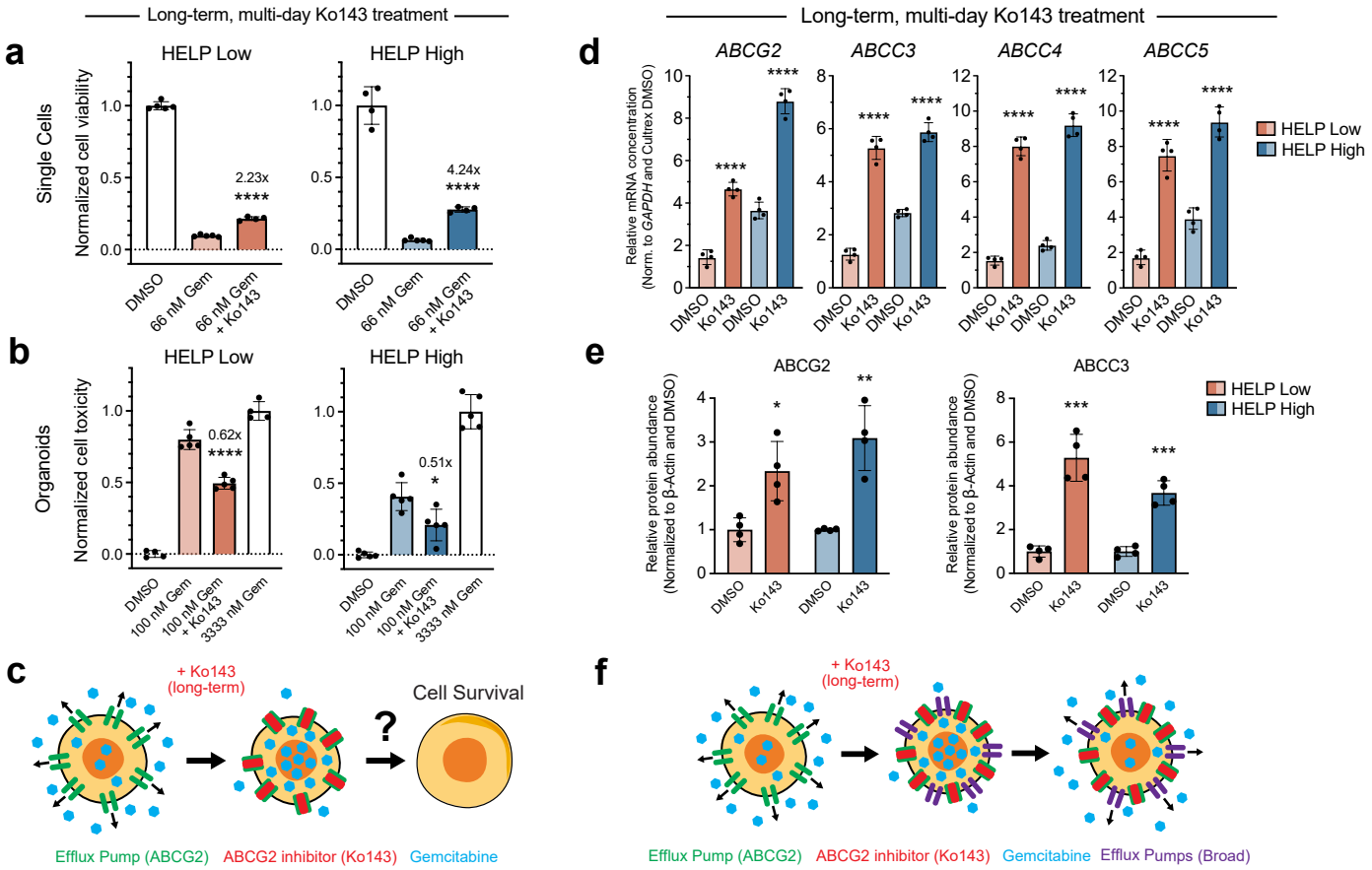

Extended Data Fig. 2 | Long-term drug efflux inhibitor treatment exacerbates PDAC organoid chemoresistance. a, PDAC viability following treatment with DMSO (control, normalized to 1), 66 nM gemcitabine (Gem), or 66 nM gemcitabine + 20 μM Ko143 (N = 4-5 independent experimental replicate hydrogels, mean ± s.d.). **b**, PDAC toxicity following treatment with DMSO (control, normalized to 0), 100 nM gemcitabine, 100 nM gemcitabine + 20 μM Ko143, or 3,333 nM gemcitabine (positive control, normalized to 1) (N = 4-5 independent experimental replicate hydrogels, mean ± s.d.). In **a** and **b**, PDAC organoids were expanded for four passages in HELP Low (left) or HELP High (right) prior to gemcitabine (+ Ko143) treatment for six days on single cells during log-phase growth (**a**) or for three days following formation of ~75-μm diameter multicellular organoids (**b**). Statistical analysis comparing experimental gemcitabine treatment and gemcitabine + Ko143 treatment was performed using an unpaired two-tailed t-test (*P < 0.05, ****P < 0.0001), and the fold change between these two conditions is reported for each comparison. **c**, Illustrated summary of results from **a** and **b**. **d**,**e**, qPCR (**d**) and Western blot (**e**) quantification of mRNA and protein-level ABC-family drug efflux transporter expression in PDAC organoids expanded within HELP Low or HELP High for four passages and treated with either DMSO or 20 μM Ko143 (N = 4 independent experimental replicates, qPCR: mean ± 95% confidence interval, Western: mean ± s.d.). Statistical analysis comparing DMSO vs. Ko143 treatment for each matrix was performed using an unpaired two-tailed t-test (*P < 0.05, **P < 0.01, ***P < 0.001, ****P < 0.0001). qPCR data are normalized to *GAPDH* gene expression and respective marker expression of Cultrex DMSO samples. Western data are normalized to β-actin expression and DMSO samples for each marker and matrix. PDAC cells were treated with Ko143 throughout single-cell log-phase growth for six days. **f**, Illustrated summary of results from **d** and **e**.

https://doi.org/10.1038/s41563-024-01908-x

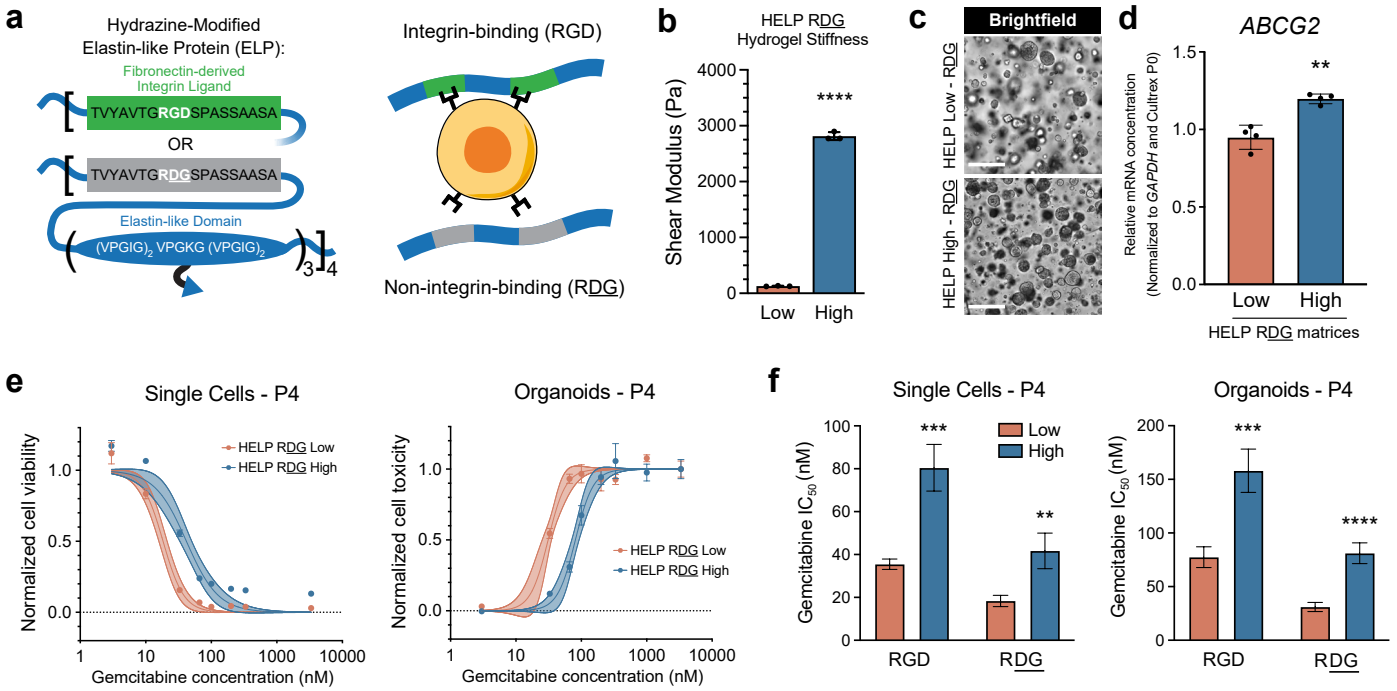

Extended Data Fig. 3 | Influence of RGD ligand on PDAC organoid chemoresistance. a, Schematic of recombinant elastin-like protein (ELP) component of HELP, which can be engineered to display a non-interactive, scrambled RDG sequence, resulting in a HELP matrix without RGD, but with identical mechanical properties and HA concentration. **b**, Stiffness measurements of HELP RDG matrices stiffness-matched to HELP Low and HELP High ($N = 3$ independent experimental replicate hydrogels, mean ± s.d., unpaired two-tailed t-test, $^{****}P < 0.0001$). **c**, Representative bright-field images of PDAC organoids expanded within HELP RDG Low (top) or HELP RDG High (bottom) for four passages. Scale bar, 250 µm. **d**, qPCR quantification of mRNA-level *ABCG2* expression in PDAC organoids expanded within HELP RDG Low or High for four passages ($N = 4$ independent experimental replicate hydrogels, mean ± 95% confidence interval). Statistical analysis comparing marker expression in Low vs. High matrices was performed using an unpaired two-tailed t-test ($^{**}P < 0.01$). All data are normalized to *GAPDH* gene expression and respective marker expression in the PDAC organoid parent population cultured within Cultrex prior to expansion in HELP RDG (that is, Cultrex P0). **e**, Single-cell-level (left) and organoid-level (right) gemcitabine dose-response curves for PDAC organoids expanded within HELP RDG Low or High for four passages. Each data point represents the mean ± s.e.m. ($N = 4$ independent experimental replicate hydrogels, solid center line is nonlinear least squares regression of data; shaded region represents 95% confidence bands of nonlinear fit; data are normalized to positive controls (DMSO for single cells, 3,333 nM gemcitabine for organoids). **f**, Gemcitabine IC_{50} values calculated from nonlinear fit of dose-response curves shown in **e** for single-cell (left) and organoid (right) drug treatment in HELP RDG compared to HELP containing RGD. Each bar represents the mean ± s.e.m. ($N = 4$ independent experimental replicate hydrogels, unpaired two-tailed t-test between Low and High for each matrix variation, $^{**}P < 0.01$, $^{***}P < 0.001$, $^{****}P < 0.0001$).

nature portfolio

Corresponding author(s): Sarah Heilshorn

Last updated by author(s): Apr 6, 2024

Reporting Summary

Nature Portfolio wishes to improve the reproducibility of the work that we publish. This form provides structure for consistency and transparency in reporting. For further information on Nature Portfolio policies, see our Editorial Policies and the Editorial Policy Checklist.

Statistics

For all statistical analyses, confirm that the following items are present in the figure legend, table legend, main text, or Methods section.

n/a	Confirmed	
☐	☒	The exact sample size (*n*) for each experimental group/condition, given as a discrete number and unit of measurement
☐	☒	A statement on whether measurements were taken from distinct samples or whether the same sample was measured repeatedly
☐	☒	The statistical test(s) used AND whether they are one- or two-sided *Only common tests should be described solely by name; describe more complex techniques in the Methods section.*
☒	☐	A description of all covariates tested
☐	☒	A description of any assumptions or corrections, such as tests of normality and adjustment for multiple comparisons
☐	☒	A full description of the statistical parameters including central tendency (e.g. means) or other basic estimates (e.g. regression coefficient) AND variation (e.g. standard deviation) or associated estimates of uncertainty (e.g. confidence intervals)
☐	☒	For null hypothesis testing, the test statistic (e.g. *F*, *t*, *r*) with confidence intervals, effect sizes, degrees of freedom and *P* value noted *Give P values as exact values whenever suitable.*
☒	☐	For Bayesian analysis, information on the choice of priors and Markov chain Monte Carlo settings
☒	☐	For hierarchical and complex designs, identification of the appropriate level for tests and full reporting of outcomes
☐	☒	Estimates of effect sizes (e.g. Cohen's *d*, Pearson's *r*), indicating how they were calculated

Our web collection on statistics for biologists contains articles on many of the points above.

Software and code

Policy information about availability of computer code

Data collection	THUNDER Imager 3D Cell Culture DMi8 epifluorescent microscope (Leica Microsystems) and LAS X software (v.3.7.5.24914) was used to acquire images of stained or unstained organoids and tissues. SPE DMI 4000B confocal microscope (Leica Microsystems) and LAS X software (v.3.5.6.21594) was used to acquire images of stained organoids and tissues. Ti2-E inverted microscope (Nikon) equipped with a confocal scanning head (Nikon, C2) and an oil immersion objective (Nikon, CFI Apochromat TIRF 100XC) was used to acquire coherent anti-Stokes Raman scattering (CARS) images of engineered matrices. Comparison of normal vs. tumor gene expression was collected from The Cancer Genome Atlas dataset and The Genotype Tissue Expression Project dataset via a previously published online tool (http://gepia.cancer-pku.cn/index.html). AR-G2 rheometer (TA Instruments) and Trios software (v.4.1.0.31739) was used to acquire stiffness measurements of hydrogels and tissue samples. 500 MHz NMR spectrometer (Varian Inova console) and VNMRJ software (v.4.2) was used to acquire NMR data on all polymer and small molecules. BD FACS Symphony A5 or A6 Sorter (BD Biosciences) and BD FACSDiva software (v.9.1) was used to acquire flow cytometry and cell cycle analysis data, and for running FACS. LUMIstar Omega luminometer (BMG Labtech) and Omega software (v.5.10 R2) was used to acquire drug dose response data. StepOnePlus Real Time PCR System (Applied Biosystems) and StepOne software (v.2.3) was used to acquire qPCR data and Ct values. ChemiDoc MP Imaging Systems (BioRad) and ImageLab software (BioRad; v.6.0) was used to acquire Western blot images. NanoDrop 2000c Spectrophotometer (Thermo Scientific) and NanoDrop 2000c software (v.1.6.198) and was used to quantify mRNA concentrations for qPCR workflow. Illumina MiSeq (Illumina) was used to acquire DNA barcode sequencing data.
Data analysis	ImageJ/FIJI (NIH, v.2.1.0/1.53c) was used for image processing, analysis, and visualization. GraphPad Prism (v.9.3.1) was used for data visualization, statistical analysis, and IC50 dose response curve analysis. MestReNova (v.14.2.3-29241) was used for all visualization and quantification of NMR spectra.

Barcode DNA sequencing FASTQ data were analyzed with an output of read counts per unique barcode using python and R (v4.0.1). Detailed information on procedures can be found here: https://www.biorxiv.org/content/10.1101/2022.04.09.487529v2.
MATLAB (v.9.11.0.1769968) was used for data normalization and visualization of DNA barcode read counts.
FlowJo (v.10.7.1) was used for analysis of all flow cytometry data.
Fluorescence recovery after photobleaching (FRAP) analysis was performed using an open source MATLAB code called 'frap_analysis'. More details can be found here: Jönsson, P., Jonsson, M. P., Tegenfeldt, J. O. & Höök, F. A method improving the accuracy of fluorescence recovery after photobleaching analysis. Biophysical Journal 95, 5334–5348 (2008).
ImageLab software (BioRad; v.6.0) was used for visualization and quantification of Western blots.
The ICE analysis tool from Synthego (https://ice.synthego.com/#/) (v.3.0) was used to verify the cut-site and estimate KO efficiency.

For manuscripts utilizing custom algorithms or software that are central to the research but not yet described in published literature, software must be made available to editors and reviewers. We strongly encourage code deposition in a community repository (e.g. GitHub). See the Nature Portfolio guidelines for submitting code & software for further information.

Data

Policy information about availability of data

All manuscripts must include a data availability statement. This statement should provide the following information, where applicable:

- Accession codes, unique identifiers, or web links for publicly available datasets
- A description of any restrictions on data availability
- For clinical datasets or third party data, please ensure that the statement adheres to our policy

All data needed to evaluate the conclusions in the paper are present in the manuscript and/or the Supplementary Information. Raw data related to this paper are uploaded to the Stanford Digital Repository, which can be accessed through the persistent URL (https://purl.stanford.edu/nw595bg6402) and the DOI (https://doi.org/10.25740/nw595bg6402). RNA-sequencing data from the TCGA and GTEx databases was accessed and plotted using the GEPIA online tool (http://gepia.cancer-pku.cn).

Field-specific reporting

Please select the one below that is the best fit for your research. If you are not sure, read the appropriate sections before making your selection.

☒ Life sciences ☐ Behavioural & social sciences ☐ Ecological, evolutionary & environmental sciences

For a reference copy of the document with all sections, see nature.com/documents/nr-reporting-summary-flat.pdf

Life sciences study design

All studies must disclose on these points even when the disclosure is negative.

Sample size	We did not perform any specific calculations to determine sample size within this study. For most analyses, we found n=4 independently prepared replicate hydrogels per condition were sufficient to accurately represent the reproducibility of the results. All samples sizes, statistical tests, and p-values are described in the figure captions. Previously published articles using similar methods to assess similar outcomes also served as a guide for determining sample sizes for each experiment (references: 19, 25-30).
Data exclusions	No data acquired for quantitative analysis was excluded from the study.
Replication	Each experiment in this study was performed with at least 3-4 independent biological replicates. Additionally, the majority of findings within this work were replicated and validated using several orthogonal methodologies (e.g., marker expression in our different hydrogels was assayed via qPCR (mRNA), immunostaining (protein), and flow cytometry (protein); drug response to gemcitabine treatment was assayed via quantification of immunostaining as well as using two distinct multiwell plate based assays upon treatment at two distinct timepoints throughout organoid development from single cells to multicellular clusters; drug transporter expression was assayed using qPCR (mRNA), Western blot (protein), flow cytometry (protein levels/activity), and immunostaining (protein)). Each attempt at replication resulted in similar outcomes. Similar trends in chemoresistance were observed across 3 PDAC patient organoid lines used in this study.
Randomization	The allocation of organoid samples into all control and experimental groups was random.
Blinding	The same researchers who set-up or ran the experiments were the same researchers to perform the data analysis. As a result, most experiments were not blinded. As an exception, the images that were quantified for cleaved caspase-3 expression were all blinded to the researcher by a different researcher prior to analysis.

Reporting for specific materials, systems and methods

We require information from authors about some types of materials, experimental systems and methods used in many studies. Here, indicate whether each material, system or method listed is relevant to your study. If you are not sure if a list item applies to your research, read the appropriate section before selecting a response.

Materials & experimental systems

n/a	Involved in the study
☐	☒ Antibodies
☐	☒ Eukaryotic cell lines
☒	☐ Palaeontology and archaeology
☒	☐ Animals and other organisms
☐	☒ Human research participants
☒	☐ Clinical data
☒	☐ Dual use research of concern

Methods

n/a	Involved in the study
☒	☐ ChIP-seq
☐	☒ Flow cytometry
☒	☐ MRI-based neuroimaging

Antibodies

Antibodies used

Primary antibodies for immunostaining:
Anti-ABCG2/BCRP1 (Rabbit, Cell Signaling 42078S, 1:200)
Anti-CD44 (Mouse, Santa Cruz Biotech sc7297, 1:50)
Anti-Cleaved caspase-3 (Rabbit, Cell Signaling 9664S, 1:400)
Anti-Cytokeratin 19 (Rabbit, Abcam ab52625, 1:200)
Anti-Fibronectin (Rabbit, Cell Signaling 26836S, 1:200)
Anti-Ki67 (Rabbit, Cell Signaling 9129S, 1:200)
Anti-Ki67 (Mouse, Cell Signaling 9449S, 1:200)

Primary antibodies for flow cytometry:
Anti-ABCG2/BCRP1 (PE-conjugated, Mouse, Invitrogen 12-8888-42, 5:100)
Anti-CD44 (APC-conjugated, Rat, Invitrogen 17-0441-81, 0.15:100)

Primary antibodies for Western Blot:
Anti-ABCC3/MRP3 (Rabbit, Cell Signaling 14182S, 1:1000)
Anti-ABCG2/BCRP1 (Rabbit, Cell Signaling 42078S, 1:1000)
Anti-β-Actin (Rabbit, Cell Signaling 4970S, 1:1000)

Secondary antibodies for immunostaining:
goat-anti-mouse (AF488, Invitrogen A11029, 1:500)
goat-anti-mouse (AF647, Invitrogen A21237, 1:500)
goat-anti-mouse (AF532, Invitrogen A11002, 1:500)
goat-anti-rabbit (AF488, Invitrogen A11034, 1:500)
goat-anti-rabbit (AF546, Invitrogen A11071, 1:500)
goat-anti-rabbit (AF647, Invitrogen A32733, 1:500)

Secondary antibodies for Western Blot:
donkey-anti-rabbit (HRP-conjugated, JacksonImmuno Research 711-035-152, 1:10,000)

Other reagents for immunostaining:
DAPI (5 mg/mL stock in water, MilliporeSigma D9542, 1:2000)
Phalloidin (100 ug/mL stock in DMSO, MilliporeSigma P1951 / P5282, 1:500)
Biotinylated Hyaluronan Binding Protein (500ug/mL stock in water, MilliporeSigma 38591150UG, 1:100)
Streptavidin (1 mg/mL in PBS, AF488, Invitrogen S11223, 1:500)

Validation

Background signal was assessed using secondary antibody-only controls for staining of whole mount organoids in hydrogels and staining of tissues/organoids that were paraffin embedded and sectioned. The manufacturers provided validation for each antibody (see below).

Primary antibodies for immunostaining:
Anti-ABCG2/BCRP1 (https://www.cellsignal.com/products/primary-antibodies/abcg2-d5v2k-xp-rabbit-mab/42078)
Anti-CD44 (https://www.scbt.com/p/hcam-antibody-df1485)
Anti-Cleaved caspase-3 (https://www.cellsignal.com/products/primary-antibodies/cleaved-caspase-3-asp175-5a1e-rabbit-mab/9664)
Anti-Cytokeratin 19 (https://www.abcam.com/cytokeratin-19-antibody-ep1580y-cytoskeleton-marker-ab52625.html)
Anti-Fibronectin (https://www.cellsignal.com/products/primary-antibodies/fibronectin-fn1-e5h6x-rabbit-mab/26836)
Anti-Ki67 (Rabbit, https://www.cellsignal.com/products/primary-antibodies/ki-67-d3b5-rabbit-mab/9129)
Anti-Ki67 (Mouse, https://www.cellsignal.com/products/primary-antibodies/ki-67-8d5-mouse-mab/9449)

Primary antibodies for flow cytometry:
Anti-ABCG2/BCRP1 (https://www.thermofisher.com/antibody/product/CD338-ABCG2-Antibody-clone-5D3-Monoclonal/12-8888-42)
Anti-CD44 (https://www.thermofisher.com/antibody/product/CD44-Antibody-clone-IM7-Monoclonal/17-0441-82)

Primary antibodies for Western Blot:
Anti-ABCC3/MRP3 (https://www.cellsignal.com/products/primary-antibodies/mrp3-abcc3-d1w1p-rabbit-mab/14182)
Anti-ABCG2/BCRP1 (https://www.cellsignal.com/products/primary-antibodies/abcg2-d5v2k-xp-rabbit-mab/42078)
Anti-β-Actin (https://www.cellsignal.com/products/primary-antibodies/b-actin-13e5-rabbit-mab/4970

Secondary antibodies for immunostaining:

goat-anti-mouse (AF488, https://www.thermofisher.com/antibody/product/Goat-anti-Mouse-IgG-H-L-Highly-Cross-Adsorbed-Secondary-Antibody-Polyclonal/A-11029)
goat-anti-mouse (AF647, https://www.thermofisher.com/antibody/product/Goat-anti-Mouse-IgG-H-L-Cross-Adsorbed-Secondary-Antibody-Polyclonal/A-21237)
goat-anti-mouse (AF532, https://www.thermofisher.com/antibody/product/Goat-anti-Mouse-IgG-H-L-Cross-Adsorbed-Secondary-Antibody-Polyclonal/A-11002)
goat-anti-rabbit (AF488, https://www.thermofisher.com/antibody/product/Goat-anti-Rabbit-IgG-H-L-Highly-Cross-Adsorbed-Secondary-Antibody-Polyclonal/A-11034)
goat-anti-rabbit (AF546, https://www.thermofisher.com/antibody/product/Goat-anti-Rabbit-IgG-H-L-Cross-Adsorbed-Secondary-Antibody-Polyclonal/A-11071)
goat-anti-rabbit (AF647, https://www.thermofisher.com/antibody/product/Goat-anti-Rabbit-IgG-H-L-Highly-Cross-Adsorbed-Secondary-Antibody-Polyclonal/A32733)

Secondary antibodies for Western Blot:
donkey-anti-rabbit (HRP-conjugated, https://www.jacksonimmuno.com/catalog/products/711-035-152)

Eukaryotic cell lines

Policy information about cell lines

Cell line source(s)	LWRN cells were purchased from ATCC (ATCC CRL3276). Human patient-derived primary cancer and normal adjacent pancreas tissue were obtained from the Stanford Tissue Bank from patients undergoing surgical resection at Stanford University Medical Center (SUMC). Procedures for generation of human organoid lines from patient tissue samples were approved by the SUMC Institutional Review Board (IRB) and performed under protocol #28908. All organoid lines used in this study were derived from treatment-naïve pancreatic tumors (Supplementary Table 3). Histological staining and mechanical testing of human tissue were deemed by the IRB to not involve human subjects as defined in U.S. federal regulation 45 CFR 46.102(f) or 21 CFR 50.3(g), as the patient samples were de-identified prior to acquisition. All samples were confirmed to be tumor or normal adjacent by pathological assessment at SUMC. Written informed consent for research was obtained from donors prior to tissue acquisition. Pancreatic cancer organoid cultures consisting of only epithelial cancer cells were generated as previously described: Neal, J. T. et al. Organoid Modeling of the Tumor Immune Microenvironment. Cell 175, 1972-1988.e16 (2018).
Authentication	LWRN cells (ATCC CRL3276) used to make Wnt3a, R-spondin, and Noggin conditioned medium were authenticated at the time of purchase from ATCC. Pancreatic cancer organoids were generated as described above from a primary tissue donation at the Stanford University Medical Center. The tissue samples were processed by the Stanford Tissue Bank and tumor tissue pathological assessment and validation was performed at the Stanford University Medical Center. Pancreatic cancer organoid cultures were validated to contain only epithelial cancer cells via morphological assessment and immunostaining.
Mycoplasma contamination	Pancreatic cancer organoids and LWRN cells were regularly tested for mycoplasma contamination using a MycoAlert Mycoplasma Detection Kit (Lonza LT07-318) and a Lucetta Single Tube Luminometer (Lonza AAL-1001) and tested negative.
Commonly misidentified lines (See ICLAC register)	No cells used in this study are commonly misidentified lines.

Human research participants

Policy information about studies involving human research participants

Population characteristics	The pancreatic cancer organoid lines used in this study were derived from treatment-naïve tumors from male and female patients in an age range from 27-69. More information on patients and specific attributes can be found in Supplementary Table 3. Analysis of RNA-sequencing (RNA-seq) data was performed using data collected from TCGA and The Genotype Tissue Expression Project (GTEx). The pancreatic adenocarcinoma ("PAAD") dataset was used.
Recruitment	Pancreatic cancer and normal pancreas tissue samples were collected from surgical resections from patients by the Stanford Tissue Bank. Written informed consent for research was obtained from donors prior to tissue acquisition.
Ethics oversight	Procedures for generation of human organoid lines from patient tissue samples were approved by the SUMC Institutional Review Board (IRB) and performed under protocol #28908. Histological staining and mechanical testing of human tissue were deemed by the IRB to not involve human subjects as defined in U.S. federal regulation 45 CFR 46.102(f) or 21 CFR 50.3(g), as the patient samples were de-identified prior to acquisition.

Note that full information on the approval of the study protocol must also be provided in the manuscript.

Flow Cytometry

Plots

Confirm that:

☒ The axis labels state the marker and fluorochrome used (e.g. CD4-FITC).

☒ The axis scales are clearly visible. Include numbers along axes only for bottom left plot of group (a 'group' is an analysis of identical markers).

☒ All plots are contour plots with outliers or pseudocolor plots.

☒ A numerical value for number of cells or percentage (with statistics) is provided.

Methodology

Sample preparation	Side population assay and cell cycle analysis: PDAC organoids expanded within Cultrex or HELP matrices were collected and dissociated into single cells as above. Single cells were immediately resuspended in warm complete WENR media supplemented with 5% FBS and 10 µM Y27632 (Cayman Chemical 10005583) solubilized in water at a density of 106 cells/mL. Hoechst 33342 (Thermo Fisher H3570) was added to all conditions at a concentration of 5 µg/mL, and Ko143 (200 nM; Cayman Chemical 15215) or verapamil (50 µM; Sigma V4629) solubilized in water were added to inhibition samples. Ko143 was first solubilized in DMSO at 10 µM and then diluted in PBS to 4 µM before being added to the media at a final concentration of 200nM. Samples were immediately moved to 37 °C for 2 hours, with gentle mixing every 15 min to reduce cell settling. After treatment, cell pellets were collected (5 min, 500 x g) and resuspended in ice-cold flow buffer (PBS + 5% FBS) with 7-AAD viability dye (5:100; Thermo Fisher, 00-6993-50) and immediately used for flow cytometry on a BD FACS Symphony A5. The flow rate was kept to below 200 events per second and a minimum of 50,000 live, single cell events were recorded for each sample. Side population was detected using a 428/31 band-pass filter (Hoechst-Blue) and a 670/30 band-pass and 635 long-pass filter (Hoechst-Red); excitation with a UV (305 nm) laser. Verapamil samples were used to confirm gating strategy for identification of the side population. DNA content for cell cycle analysis was detected using a 428/31 band-pass filter and excited with a UV (305 nm) laser. Cells in S phase were identified as 2n<DNA<4n. All flow cytometry analysis was performed with FlowJo software (v.10.7.1). For sorting of side population, G0/G1, and viable cells, collection was performed on a FACSymphony S6 Sorter following the same protocol as above. Flow cytometry: PDAC organoids expanded within Cultrex or HELP matrices were collected and dissociated into single cells as above. Single cells were immediately resuspended in ice-cold flow buffer (PBS + 5% FBS) with Fc receptor block (20:100; Thermo Fisher 14-9161-73). After 20 min, samples were stained for surface protein expression for 30 min on ice. Samples were washed in ice-cold flow buffer and pelleted (5 min, 500 x g). Samples were resuspended in flow buffer with 7-AAD viability dye (5:100; Thermo Fisher 00-6993-50) and immediately used for flow cytometry on a BD FACS Symphony A5. A minimum of 50,000 live, single cell events were recorded for each sample. Compensation was set using UltraComp eBeads Compensation Beads (Thermo Fisher 01-2222-41) and unstained cells. Fluorescence minus one (FMO) controls were used to set gating strategies. All antibody stains were titrated prior to use to identify optimal concentration for separation of negative and positive populations. See Supplementary Table 4 for antibodies and dilutions. All flow cytometry analysis was performed with FlowJo software (v.10.7.1). All values are reported as the median intensity of the live population.
Instrument	BD FACS Symphony A5 (BD Biosciences) or BD FACS Symphony A6 (BD Biosciences)
Software	All flow cytometry analysis was performed with FlowJo v.10.7.1
Cell population abundance	At least 50,000 cells were acquired for each condition.
Gating strategy	For all cell analysis, events were first gated for cells on FSC-A/SSC-A. Doublets were excluded by gating for single cells on FSC-A/FSC-H. This population was then used to identify live cells by gating on FSC-A/7-AAD. From this Live population, all other populations were identified. Gating for surface markers was identified using Fluorescence minus-one (FMO) controls. Side population gating was confirmed with a Verapamil control.

☒ Tick this box to confirm that a figure exemplifying the gating strategy is provided in the Supplementary Information.